KeAi

CHINESE ROOTS
GLOBAL IMPACT

Contents lists available at ScienceDirect

Petroleum Science

journal homepage: www.keaipublishing.com/en/journals/petroleum-science



Original Paper

Characteristics, preservation mechanisms, and significance of aragonite in lacustrine shale: A case study from the Jiyang Depression, Bohai Bay Basin



Zhou-Hai Xiong $^{a, b, *}$, Ying-Chang Cao $^{b, c}$, Song Xue d , Guan-Min Wang $^{b, c, **}$, Chao Liang b , Ke-Yu Liu $^{b, c}$

- ^a School of Earth Science and Engineering, Xi'an Shiyou University, Xi'an, 710065, Shaanxi, China
- ^b State Key Laboratory of Deep Oil and Gas, China University of Petroleum (East China), Qingdao, 266580, Shandong, China
- c Laboratory for Marine Mineral Resources, Qingdao National Laboratory for Marine Science and Technology, Qingdao, 266071, Shandong, China
- ^d Exploration and Development Research Institute, Jilin Oilfield Company, PetroChina, Songyuan, 138000, Jilin, China

ARTICLE INFO

Article history: Received 13 November 2023 Received in revised form 19 March 2024 Accepted 23 May 2024 Available online 24 May 2024

Edited by Jie Hao and Meng-Jiao Zhou

Keywords: Fine-grained sedimentary rocks Shale oil Aragonite Sedimentation Diagenesis

ABSTRACT

Aragonite is a metastable mineral, which is easily transformed into calcite, and generally difficult to preserve in the stratum. However, large amounts of aragonites were found in the Paleogene shale of the livang Depression. The characteristics and preservation mechanisms of these aragonites were analyzed through a series of analytical methods, including cathodoluminescence, field-emission scanning electron microscopy (FESEM), laser ablation inductively coupled plasma mass spectrometry (LA-ICP-MS), microarea carbon and oxygen isotopes, Sr isotopes, and dissolution simulation experiments under high temperature and high pressure. The research results show that: ①Aragonite in the Paleogene shale of the liyang Depression is related to algal microbial fossils, primarily composed of coccoliths and characterized by two emission peaks at 420 nm and 480 nm in cathodoluminescence; @The primary factor allowing biological aragonite to be preserved is the immaturity of the organic matter and the deficiency of abundant organic acids necessary for its dissolution or transformation, which is confirmed by the evidence of organic matter maturity and simulation experiments of organic acid dissolution on aragonite under high-temperature and high-pressure conditions. Additional factors that may aid in the preservation of aragonite are the ideal sedimentation conditions, the defense of organic coating, and the enclosed environment with tiny pores, low porosity, and low permeability; 3These aragonite-rich shales, characterized by coccolithophores, provide a solid evidence for seawater intrusion into terrestrial lake basin, and have a significant implication for the source and storage of shale oil.

© 2024 The Authors. Publishing services by Elsevier B.V. on behalf of KeAi Communications Co. Ltd. This is an open access article under the CC BY-NC-ND license (http://creativecommons.org/licenses/by-nc-nd/4.0/).

1. Introduction

Aragonite, a metastable mineral, is easily transformed into calcite or dissolved after precipitation (Brachert and Dullo, 2000; James et al., 2005; Dix and Nelson, 2006; Burdige et al., 2010; Drupp et al., 2016; Martín-García et al., 2019; Livermore et al., 2020;

E-mail addresses: xiongzhouhai@126.com (Z.-H. Xiong), wguanmin@sina.com (G.-M. Wang).

Nguyen et al., 2021; He et al., 2021; Reuning et al., 2022). Consequently, reports of aragonite are more frequent in sediments with shallow burial and less common in deeply buried shales (Munnecke et al., 2023). Specific conditions are required for aragonite to precipitate and be preserved under natural conditions, but these conditions vary significantly depending on the type of aragonite, which is also why the origin of aragonite has always been a subject of considerable controversy.

As for sedimentation, aragonite includes biological and abiotic precipitation (Jones, 2017). Most biogenic aragonites are directly related to biological skeletons (Perrin, 2004; Meibom et al., 2007; Cuif et al., 2008). For example, coral skeletons are composed of aragonites (Meibom et al., 2007). Inorganic aragonite is related to

^{*} Corresponding author. School of Earth Science and Engineering, Xi'an Shiyou University, Xi'an, 710065, Shaanxi, China.

^{**} Corresponding author. State Key Laboratory of Deep Oil and Gas, China University of Petroleum (East China), Qingdao, 266580, Shandong, China.

the type of ion component and concentration, temperature, and pH value (Wassenburg et al., 2012; Ma et al., 2017; Shiraishi et al., 2020; Christensen et al., 2021; Ben Dor et al., 2021). According to Riccioni et al. (1996), the formation of inorganic aragonite in lakes located in rift basins is influenced by seasonal variations. Specifically, (1) during humid periods, the deep lake becomes more enriched with organic matter, resulting in the formation of shale laminae rich in organic matter; (2) during dry periods, the lacustrine basin's water level decreases, causing the lake water to become salinized, which encourages the formation of evaporites and sulfate layers; and (3) re-entering a humid period, fresh lake water is injected, entering the bottom evaporites and sulfate layers through diffusion and filtration, along with the release of large amounts of CO₂ from the biodegradation of organic matter, promoting aragonite precipitation. Aragonite deposition is significantly influenced by temperature. Previous studies have indicated that, regardless of saturation level, aragonite precipitation rates at 5 °C are almost identical to those of calcite; nevertheless, at both 25 °C and 37 °C, aragonite precipitation rates are significantly faster than those of calcite (Burton and Walter, 1987). Many studies have shown that high salinity, Mg/Ca ratio and pH are conducive to the precipitation of aragonite (Wassenburg et al., 2012; Ma et al., 2017; Shiraishi et al., 2020). In most Ordovician marine settings, aragonite will be in a stable phase when the water temperature is between 21 and 23 °C and the Mg/Ca ratio is between 2.8 and 3.0 (Balthasar and Cusack, 2015; James et al., 2020). Bots et al. (2011) also found that a higher Mg/Ca ratio coupled with higher SO₄ content is more conducive to aragonite precipitation. However, some studies have found that Mg is not easily incorporated into the aragonite lattice. and the Mg content in water has little effect on the precipitation rate of aragonite (De Choudens-Sánchez and González, 2009). As a result, some researchers have also discovered that aragonite can precipitate in cases when Mg/Ca is less than 0.01 (Christensen et al., 2021). In addition, the production of aragonite in lacustrine basins is also controlled by climate and exhibits millennial-scale oscillations. Lower lake levels favor aragonite precipitation from supersaturated waters. Prolonged periods of stratification and, consequently, enhanced sulfate reduction favor aragonite preservation (Roeser et al., 2016).

As for the diagenesis, the thermodynamic stability of aragonite in near-surface environments (syndiagenetic stage) is lower than that of Mg-low calcite, leading to spontaneous transformation of aragonite to Mg-low calcite (He et al., 2020). Microbial activity, temperature, pressure, pH, and the types and concentration of ions in diagenetic fluids are the primary factors influencing the dissolution, precipitation, and preservation of aragonite during burial (Roeser et al., 2016; Facq et al., 2016; Smrzka et al., 2019; Zwicker et al., 2018; Guo et al., 2019; Pederson et al., 2020). During shallow burial, the dissolution of aragonite is mainly caused by aerobic respiration in the oxygen zone, nitrate reduction in the suboxic zone, bacterial sulfide degradation and methanogenesis in the anoxic zone (Froelich et al., 1979; Berner, 1981; Jørgensen and Kasten, 2006; Su et al., 2020; Munnecke et al., 2023). Additionally, organic matter content (Sanders, 2003; Bradbury and Turchyn, 2019), salinity (Dijkstra et al., 2017), oxygen supply (Munnecke et al., 2023), and the degree of laminar lithification (Nohl et al., 2020) all indirectly affect the dissolution of aragonite. Research has shown that the carbonate fluid produced by the dissolution in bacterial action zones can diffuse or seep into the upper part of the anaerobic zone and precipitate due to increased alkalinity (Wright and Cherns, 2016). The anaerobic methane oxidation zone, located between the sulfide degradation zone and the methane production zone, has a thickness of 10-50 cm (Reeburgh, 1983). This zone's δ^{13} C is not very light because the precipitated calcite mostly results from aragonite dissolution rather than methane oxidation as the

dominant source (Raiswell and Fisher, 2000; Bradbury and Turchyn, 2019). This is also the reason why many marine limestones have heavier δ^{13} C values (Bottrell and Raiswell, 1989). Moreover, the aragonite derived from the transformation of aragonite often has some unique characteristics. Generally, there is only a small amount of magnesium in the aragonite lattice. The dissolution of aragonite reduces the Mg/Ca ratio in pore water, and the precipitated calcite is mainly Mg-low calcite (Melim et al., 2002; Swart, 2015). This also explains why seawater has a high Mg/Ca ratio, while pore water in sediments lacks low-Mg/Ca ratio (Munnecke et al., 1997). During the diagenetic evolution of aragonite, ⁴⁴Ca is relatively depleted while ²⁶Mg is relatively enriched (Gussone et al., 2005; Higgins et al., 2018). Furthermore, during the transformation of aragonite to calcite, the released Sr from aragonite dissolution does not easily enter the calcite lattice but diffuses together with incompatible elements (such as V and Th) (Nohl et al., 2021).

To summarize, aragonite's deposition, diagenesis, or transition into calcite is a rather complicated process, particularly requiring specific diagenetic and sedimentary environments for its dissolution, precipitation, and preservation.

Large amounts of aragonites were found in the Paleogene shale of the Jiyang Depression. The Jiyang Depression, located in Shandong Province, China, belongs to a secondary tectonic unit of the Bohai Bay Basin (Wu et al., 2003; Qiu et al., 2006), including the Dongying, Huimin, Zhanhua and Chezhen Sags (Fig. 1). The Paleogene strata in the Jiyang Depression is composed of the Kongdian (Ek), Shahejie (Es) and Dongying Formations (Ed), of which the Es is further divided into 4 sub members (Es1, Es2, Es3 and Es4). The Ek and the lower Es4 (Es4x) are primarily alluvial fan deposits, the Es1, Es3 and the upper Es4 (Es4s) are lacustrine deposits, primarily mudstone, which are the primary source rocks in the Jiyang Depression, the Es2 is primarily fluvial and delta deposits, and the Ed is mainly lacustrine and alluvial fan deposits (Chen et al., 2016; Zhang et al., 2016; Liang et al., 2018). As shown in Table 1, aragonite predominantly occurs in the Es1 formation, with occasional occurrences in the mud shale of the lower Es2 (Es2x), Ed3, and upper Es3 (Es3s) formations. Why aragonites can be preserved in the formation for a long time, and what are the conditions for their transformation into calcite, are very worth considering. Therefore, we have analyzed the petrological, mineralogical and geochemical characteristics of these aragonites by using a variety of analytical techniques and methods, to reveal and understand the formation and preservation mechanisms of shale aragonites, as well as the significance in geology.

2. Samples and methodology

The samples for this study were primarily collected from the Dongying, Zhanhua, and Huimin Sags, as shown in Table 1. The aragonite-rich strata in the Dongying Sag are Es1, Es3s, and Ed3. These strata have burial depths of typically less than 2600 m and an aragonite concentration of between 25% and 40%. In the Huimin Sag, the aragonite-rich strata, Es1 and Ed3, are often found at burial depths of less than 2400 m, with concentrations varying from 30% to 65%. The Zhanhua Sag's aragonite-rich strata, Es1 and Es2x, have an aragonite concentration of 15%—60% and are often found at burial depths of less than 3300 m. To explore the characteristics and preservation mechanisms of aragonite, we selected a core from the Y51 well at a depth of 2672 m in the Es1 stratum (with a high aragonite content of up to 60%) as a representative sample for further analysis.

Various analytical techniques such as thin-section, cathodoluminescence (CL), X-ray diffraction (XRD), X-ray fluorescence (XRF), vitrinite reflectance, field-emission scanning electron

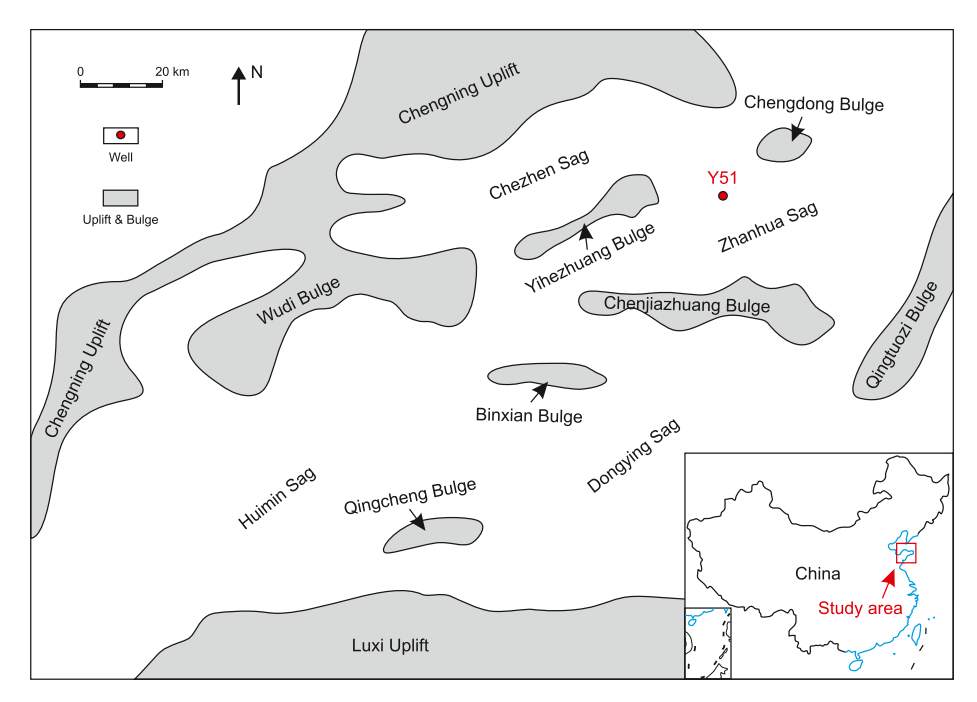


Fig. 1. Location map of the Jiyang Depression.

Table 1Mineral composition characteristics of aragonite-rich fine-grained sedimentary rocks in the Jiyang Depression.

Region	Well	Member	Depth	Aragonite, wt%	Quartz, wt%	Feldspar, wt%	Calcite, wt%	Dolomite, wt%	Pyrite, wt%	Clay mineral, wt%
Zhanhua Sag	L63	Es1	2284.50	28	26	1	8	6	3	28
	Y21	Es1	2755.40	29	36	9	7	5	0	14
			2764.00	49	18	4	10	5	0	14
			2764.04	49	18	4	10	5	1	13
			2764.94	30	31	5	9	14	0	11
			2768.70	15	17	4	48	3	0	13
			2769.00	30	19	3	33	6	0	9
	Y51	Es1	2650.00	10	24	3	3	25	2	33
			2672.00	60	13	2	3	3	3	16
			2681.60	36	20	4	18	9	0	13
	Y60	Es1	3014.97	36	26	6	9	5	1	17
			3015.90	40	27	3	6	3	1	20
			3016.57	43	23	2	5	5	2	20
			3323.45	32	32	4	8	4	0	20
	YD341	Es1	3220.10	12	23	4	42	3	1	15
			3221.60	15	30	3	15	2	3	32
	XBS1	Es2x	2910.50	10	13	5	5	37	10	20
Huimin Sag	L27-1	Es1	2411.30	30	9	5	11	10	5	30
			2412.80	30	17	8	12	8	3	22
	S20-2	Es1	1501.55	50	7	3	13	1	4	22
			1501.89	50	10	4	10	3	2	21
			1503.30	60	11	5	9	2	1	12
			1503.30	65	10	5	10	2	1	7
			1520.90	30	14	5	16	4	5	26
	X19	Ed3	1810.10	15	5	35	5	6	4	30
Dongying Sag	C23	Es1	1524.10	40	18	6	7	4	3	22
			1525.50	30	15	4	12	2	8	29
			1526.90	25	11	9	4	12	14	25
			1526.90	25	15	17	13	2	10	18
	D651	Es3s	2407.30	15	13	10	12	16	9	25
			2407.65	25	7	7	18	12	11	20
			2407.80	22	15	8	13	18	9	15
	G1	Ed3	2631.70	15	16	8	13	13	10	25
			2632.10	25	15	13	15	10	7	15

microscopy and cathodoluminescence (FESEM-CL), electron probe, LA-ICP-MS, and micro-area C, O and Sr isotope were used in the research. Based on XRD analysis, the core Y51-2672 m with high aragonite content was selected as the research object for XRF, FESEM, LA-ICP-MS and C, O, Sr isotope analysis.

FESEM-CL analysis, conducted at the State Key Laboratory of Deep Oil and Gas, China University of Petroleum (East China), was carried out by a combination of field emission scanning electron microscopy (FESEM) and cathodoluminescence (CL) system.

LA-ICP-MS analysis, involving a total of a total of 15 points, was conducted at the State Key Laboratory of Deposit Geochemistry, Institute of Geochemistry, Chinese Academy of Sciences. The analysis employed a combination of laser ablation system (GeoLasPro 193 nm ArF (Argon Fluoride) excimer laser) and ICP-MS instrument (Agilent 7900). During the laser ablation process, helium gas served as the carrier gas, argon gas functioned as the compensation gas, and a small amount of nitrogen gas was added to enhance sensitivity. These gases were mixed through a T-shaped joint before entering the ICP. The laser operated at a frequency of 7 Hz, an energy density of $4-5 \text{ J/cm}^2$, and a beam spot size of 32 μ m. Prior to testing, the ICP-MS performance was optimized using Standard Reference Material (SRM) 610 to achieve optimal sensitivity and ionization efficiency (U/Th ≈ 1), minimize oxide yield (ThO/ Th < 0.3 %), and maintain a low background level. Each collection cycle consisted of approximately 20 s of blank signal followed by 50 s of sample signal. For every 10–15 samples, NIST SRM 610 (National Institute of Standards and Technology Standard Reference Material) was analyzed twice. NIST SRM 612 was analyzed once. and after the test points. NIST SRM 612 was analyzed once again followed by 2 analyses of NIST SRM 610 (i.e., 2 NIST SRM 610 + 1 NIST SRM 612 + 10-15 test points+1 NIST SRM 612 + 2 NIST SRM 610). Sensitivity shift correction was performed using NIST 610 for analysis, while NIST 612 served as the external standard, and calcium (Ca) was used as the internal standard to correct the content of other elements. During data detection, carbonate powder compression MACS-3 (Multi-Analyte Control Set) was employed to monitor data quality. The analysis aimed for an accuracy of most elements in the results better than 10%. Recommended values for element content in calibration materials and quality control samples were based on the GeoReM database (http://georem.mpchmainz.gwdg.de/). Data processing was conducted offline using the ICPMSDataCal software.

Micro-area carbon and oxygen isotope analysis, involving a total of 7 points, was conducted at the State Key Laboratory of Deep Oil and Gas, China University of Petroleum (East China). The samples were obtained via microdrilling under a microscope, and analyzed using an instrument of Finnigan Mass Analyzer Technology (MAT) 253. The powder samples were reacted in anhydrous phosphoric acid in sealed tubes at a constant temperature of 72 °C for 2 h. The collected CO₂ was used for isotope analysis by the stable isotope ratio mass spectrometry (IRMS), and the ions with mass fractions of 44, 45 and 46 were collected by three receivers respectively. A phosphoric acid fractionation factor of 1.00986 for dolomites (Rosenbaum and Sheppard, 1986) was adopted to calculate the isotopic values. Results are expressed in the usual δ notation in %relative to V-PDB (Vienna-Pee Dee Belemnite) standard for both $\delta^{13}\text{C}$ and $\delta^{18}\text{O}.$ The data is calibrated using a set of internationally recognized reference standards NBS-18 (National Bureau of Standards 18) and IAEA-603 (International Atomic Energy Agency 603), and the standard deviations of $\delta^{13} \text{C}$ and $\delta^{18} \text{O}$ for the NBS-18 are $0.035\ \%$ and $0.1\ \%$, while $0.01\ \%$ and $0.04\ \%$ for the IAEA-603, respectively. The precision and accuracy of the isotopic measurements are estimated to be better than 0.1 %.

Micro-area Sr isotope analysis, with a total of 10 points, was conducted on a Nu Plasma III MC-ICP-MS (Nu Instruments) that was

attached to a Resolution-155 ArF193-nm laser ablation system (Australian Scientific Instruments) at State Key laboratory of Ore Deposit Geochemistry, Institute of Geochemistry, Chinese Academy of Sciences. Dolomite was ablated in a mixture of helium (350 ml/min) and nitrogen (2 ml/min) atmosphere using the following parameters: 30 s baseline time, 40 s ablation time, 64 μ m spot size, 6 Hz repetition rate and 4 J/cm² energy density. The analytical and interference correction protocol follows the method described in Ramos et al. (2004) and was fully addressed in Gao and Zhou (2013). Two in-house standards consisting of a modern-day coral (MC) every five samples and a Calcite (BC) every ten unknown samples were treated as quality control. The values of Modern Coral (MC) and Calcite (BC) is 0.709172 (Hodell et al., 1990) and 0.707920 respectively.

Furthermore, to explore the evolution characteristics of aragonite during burial diagenesis, this study also selected the aragonite-rich Y51-2672 m core and the calcite-rich Y51-2665.1 m core for high temperature and pressure dissolution experiments. The specific experimental steps are as follows: (1) Powder the two cores to between 40 mesh (0.42 mm) and 60 mesh (0.25 mm) respectively; (2) Wrap the powder sample with gauze, 10 g each, and put it into the autoclave; (3) Combined with the concentration characteristics of organic acids in the actual formation, 500 mL of 0.16 mol/L medium solution is prepared with distilled water and acetic acid as the solvent; (4) Dissolution experiments were performed under the conditions of 80 °C and 16 MPa, 100 °C and 21 MPa, 120 °C and 26 MPa, and 160 °C and 32 MPa respectively, and the reaction time was 24 h; (5) After the experiment, the ICP-MS equipment was used to detect the Ca²⁺ concentration in the reacted residual liquid.

3. Aragonite characteristics

3.1. Petrological characteristics

Aragonite is widely developed in Paleogene shale of the Jiyang Depression, especially the shale of Shahejie and Dongying Formations, as shown in Table 1. These aragonite-rich shales are mainly composed of aragonite, quartz, feldspar, clay minerals, calcite, dolomite, and pyrite. The content of aragonite varies greatly, from 0 to 65 wt%.

Y51-2672 m core, for instance, has an aragonite composition of up to 60 wt%, as indicated by the XRD diffraction spectrum displayed in Fig. 2. On the core scale, both laminar and massive aragonite-rich shales are developed, and the cathodoluminescence is primarily gray and gray-black (Fig. 3(a)). Laminar and massive structures also commonly be observed at a slice scale. Laminated aragonite-rich shale is composed of clay laminae and aragonite

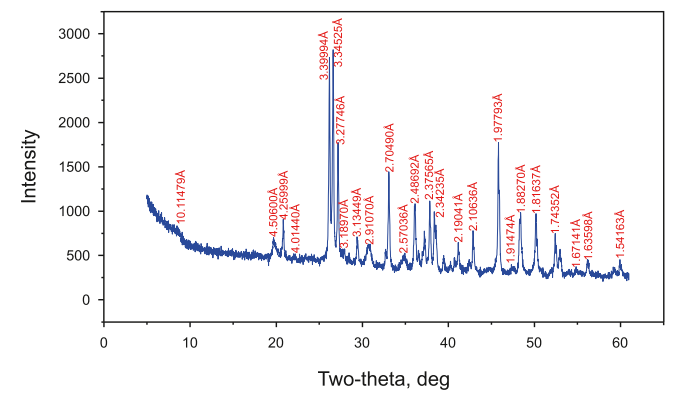


Fig. 2. The spectrum of XRD diffraction from the aragonite-rich shale (Y51-2672 m).

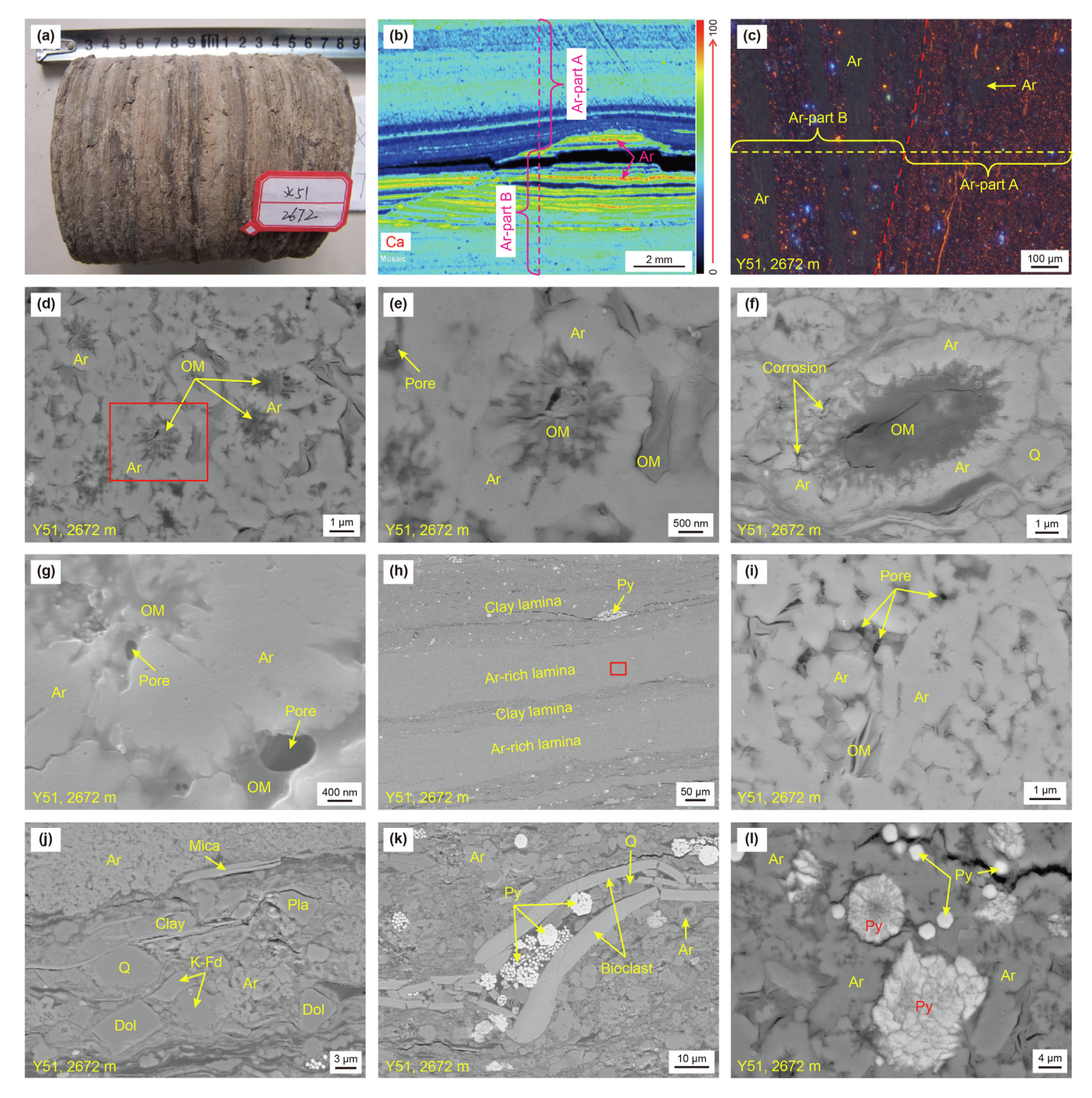


Fig. 3. Algal fossils and their surrounding rock characteristics in fine-grained sedimentary rocks.

(a) Aragonite-rich shale core, Y51, 2672 m; (b) Calcium content distribution characteristics of aragonite-rich shale, slice XRF scanning image, Y51, 2672 m; (c) Cathodoluminescence characteristics of aragonite-rich shale slice, Y51, 2672 m; (d) General characteristics of biological aragonite in massive shale, Y51, 2672 m; (e) Characteristics of individual algal fossil in massive shale, Y51, 2672 m; (f) Characteristics of ellipsoidal biological aragonite in massive shale, Y51, 2672 m; (g) Corrosion characteristics of biological aragonite in massive shale, Y51, 2672 m; (h) General characteristics of biological aragonite in laminar shale, Y51, 2672 m; (j) Characteristics of biological aragonite in laminar shale, Y51, 2672 m; (j) Characteristics of clay lamina in laminar shale, Y51, 2672 m; (k) Bioclastic characteristics in aragonite-rich shale, Y51, 2672 m; (l) Pyrite characteristics in aragonite-rich shale, Y51, 2672 m; (l) Pyrite characteristics in aragonite-rich shale, Y51, 2672 m; (l) Pyrite characteristics in aragonite-rich shale, Y51, 2672 m; (l) Pyrite characteristics in aragonite-rich shale, Y51, 2672 m; (l) Pyrite characteristics in aragonite-rich shale, Y51, 2672 m; (l) Pyrite characteristics in aragonite-rich shale, Y51, 2672 m; (l) Pyrite characteristics in aragonite-rich shale, Y51, 2672 m; (l) Pyrite characteristics in aragonite-rich shale, Y51, 2672 m; (l) Pyrite characteristics in aragonite-rich shale, Y51, 2672 m; (l) Pyrite characteristics in aragonite-rich shale, Y51, 2672 m; (l) Pyrite characteristics in aragonite-rich shale, Y51, 2672 m; (l) Pyrite characteristics in aragonite-rich shale, Y51, 2672 m; (l) Pyrite characteristics in aragonite-rich shale, Y51, 2672 m; (l) Pyrite characteristics in aragonite-rich shale, Y51, 2672 m; (l) Pyrite characteristics of biological aragonite in aragonite-rich shale, Y51, 2672 m; (l) Pyrite characteristics of biological aragonite in aragonite-rich shale, Y51

laminae, in which the aragonite laminae are composed of algal microbial fossils (Fig. 3(i)), while the clay laminae are rich in K-feldspar, plagioclase, quartz and dolomite (Fig. 3(j)). In massive aragonite-rich shale, aragonite is mixed with clay minerals, and bioclastic, quartz and pyrite are also developed in large quantities (Fig. 3(k)–(I)). In addition, it is commonly observed an erosion

surface between the laminar and massive sections (Fig. 3(b)–(c)).

3.2. Mineralogical characteristics

Most of the aragonites in massive shale are preserved as relative intact algal fossils, especially the coccolithophores, including

spherical, ellipsoid, and spindle shapes (Fig. 3(d)–(f)). The outer part of coccolithophore is composed of coccolith ring and the inner part is filled with organic matter or algae body. The coccoliths near the organic matter are commonly observed to be corroded, and dissolution pores are developed (Fig. 3(g)). Aragonite rarely exists in the form of intact coccolithophores in laminar shale, but is stacked with coccoliths (Fig. 3(h)). In addition, the pores between the coccoliths are often filled by organic matter or algae body (Fig. 3(i)). Just as the coccoliths in massive shale, dissolution features within or between coccoliths in laminar shale are also commonly observed, and dissolution pores are observed (Fig. 3(i)).

In general, the cathodoluminescence of aragonite is yellow, but the cathodoluminescence of biological aragonite is dark-brown color, as shown in Fig. 2(c). In the characteristics of the cathodoluminescence spectrum of scanning electron microscope, the

excitation peak of aragonite is obviously different from that of micritic calcite (Fig. 4). In the wavelength range of 250-800 nm, the aragonite in the laminar and massive shale primarily has two excitation peaks at 420 nm and 480 nm, and the main peak is 420 nm (Fig. 4(a)–(f)). Micritic calcite primarily has excitation peaks at 370 nm and 630 nm, and the main peak is 370 nm (Fig. 4(g)–(i)).

3.3. Geochemical characteristics

There are both similarities and differences in the geochemical characteristics of laminar and massive aragonite-rich shale. As shown in Fig. 5(a)—(b) and Table 2, the content of major elements detected by the electron probe and LA-ICP-MS data shows that the content of SiO₂, Al₂O, K₂O, MgO, FeO, TiO₂ and MnO in massive

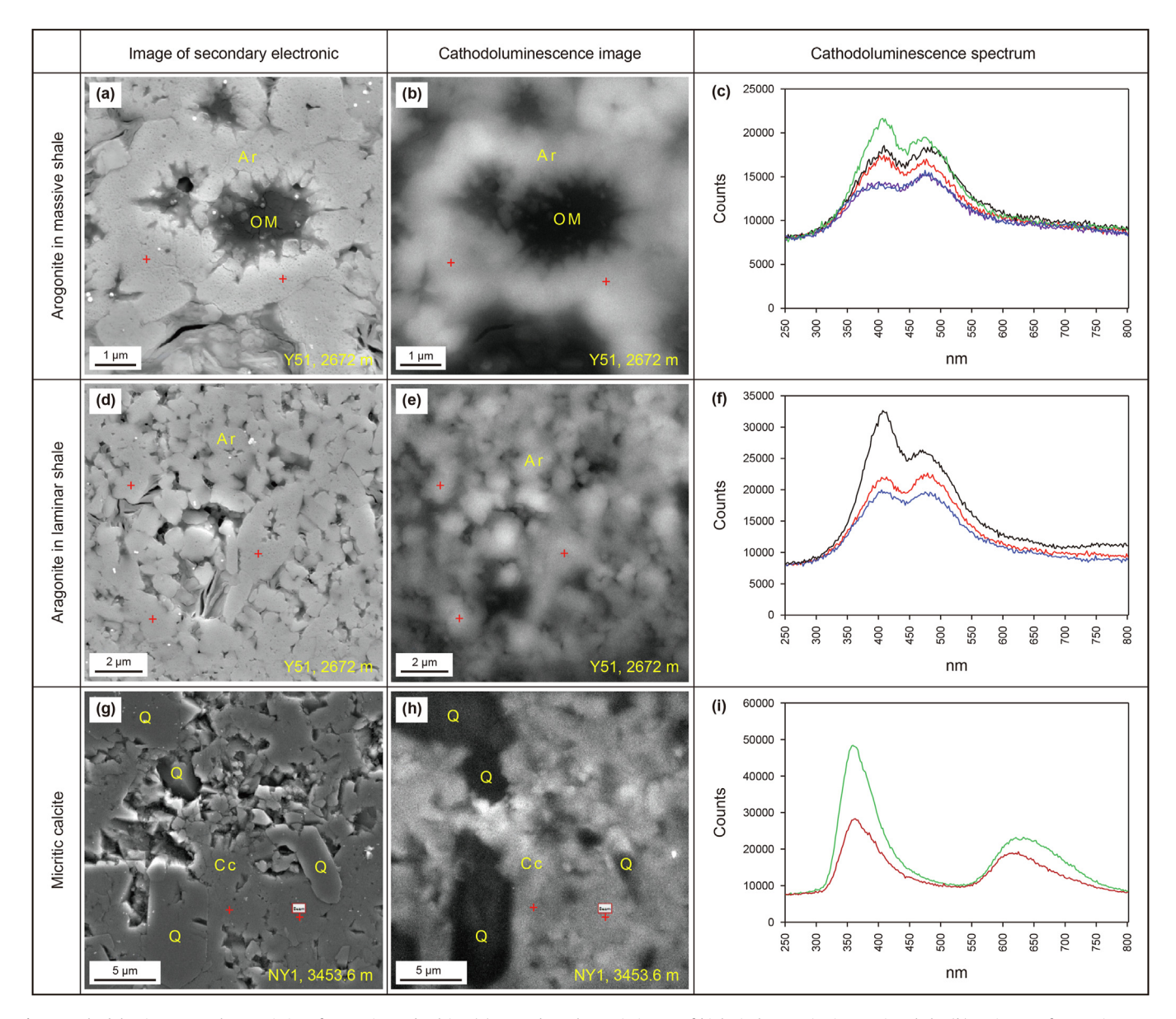


Fig. 4. Cathodoluminescence characteristics of aragonite and calcite. (a) Secondary electronic image of biological aragonite in massive shale. (b) CL image of aragonite corresponding to image (a). (c) The CL spectra corresponding to the red dot (aragonite) in images (a) and (b). (d) Secondary electronic image of biological aragonite in laminar shale. (e) CL image of aragonite corresponding to image (d). (f) The CL spectra corresponding to the red dot (aragonite) in images (d) and (e). (g) Secondary electronic image of micritic calcite. (h) CL image of calcite corresponding to image (g). (i) The CL spectra corresponding to the red dot (calcite) in images (g) and (h). Ar—aragonite; OM—organic matter; Q—quartz; Cc—calcite.

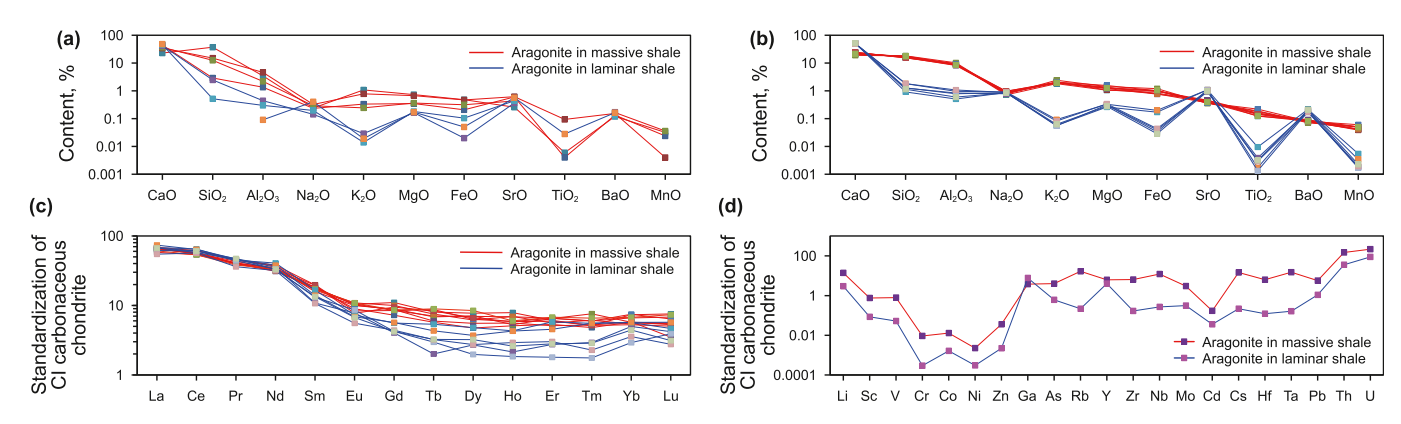


Fig. 5. Geochemical characteristics of laminar and massive aragonite.
(a) Distribution characteristics of major elements detected by electron probe microanalysis. (b) Distribution characteristics of major elements detected by LA-ICP-MS. (c) Distribution characteristics of rare earth elements. (d) Distribution characteristics of trace elements.

Table 2Major element characteristics of aragonite in massive shale (A) and laminar shale (B).

3		O	`	,	` ,						
Number	Na ₂ O, %	MgO, %	Al ₂ O ₃ , %	SiO ₂ , %	K ₂ O, %	CaO, %	TiO ₂ , %	MnO, %	FeO, %	SrO, %	BaO, %
A1	0.7140	1.0460	9.4684	15.2910	1.8107	24.1454	0.1220	0.0509	0.9584	0.4572	0.0889
A2	0.8310	1.2697	8.9835	17.9644	1.9512	20.3507	0.1894	0.0416	0.9980	0.3838	0.0755
A3	0.8079	1.0786	9.0608	16.7903	2.0219	22.2904	0.1476	0.0385	0.8273	0.4313	0.0819
A4	0.7595	1.4245	10.1792	18.1194	2.3961	18.9183	0.1820	0.0501	1.1957	0.3530	0.0709
A5	0.8370	1.2145	8.1566	15.8789	1.9731	23.9797	0.1563	0.0417	0.7600	0.4626	0.0914
A6	0.8741	1.3561	8.6473	16.5981	1.9933	22.5479	0.1590	0.0415	0.7775	0.3745	0.0792
A7	0.9449	1.5613	9.2182	16.7553	2.0577	21.3999	0.2192	0.0600	0.9967	0.3688	0.0804
A8	0.9821	1.2626	8.5265	15.3333	1.9237	24.2506	0.1428	0.0500	0.9860	0.4042	0.0816
A9	0.8963	1.2472	8.5008	17.3417	1.9631	21.5397	0.1264	0.0488	1.0244	0.3885	0.0800
B1	0.7836	0.3080	0.8335	1.2550	0.0000	51.0407	0.0038	0.0018	0.0393	0.9370	0.1869
B2	0.8656	0.2597	0.5049	0.9138	0.0570	51.4480	0.0095	0.0054	0.1703	1.0810	0.2146
B3	0.9150	0.3271	0.9560	1.8086	0.0923	49.8074	0.0017	0.0034	0.1983	1.0845	0.2067
B4	0.8596	0.3102	0.7806	1.2732	0.0552	50.8954	0.0013	0.0017	0.0334	1.0731	0.1810
B5	0.8787	0.3374	1.0712	1.8061	0.0819	49.9755	0.0029	0.0019	0.0438	1.0075	0.1685
B6	0.8392	0.2757	0.5988	1.1380	0.0622	51.3240	0.0032	0.0023	0.0286	0.9470	0.2048
Average for A	0.8496	1.2734	8.9713	16.6747	2.0101	22.1581	0.1605	0.0470	0.9471	0.4026	0.0811
Average for B	0.8569	0.3030	0.7908	1.3658	0.0581	50.7485	0.0037	0.0028	0.0856	1.0217	0.1938

shale is higher than that of laminar shale, while the content of CaO, Na_2O , SrO, and BaO in laminar shale is close to or higher than that of massive shale. In addition, the SrO content is well correlated with the aragonite content (Fig. 6(a)).

As for the characteristics of rare earth elements, the content of light rare earth elements in aragonite of massive and laminar shale is higher than that of heavy rare earth elements, which is generally

characterized by a right dip (Fig. 5(c)); however, the content of light rare earth elements in laminar shale is slightly higher than that in massive shale, while the content of heavy rare earth elements is just the opposite, much lower in the laminar shale than the massive shale (Table 3 and Fig. 5(c)).

In terms of trace element characteristics, the variation trends of trace element content characteristics of massive and laminar

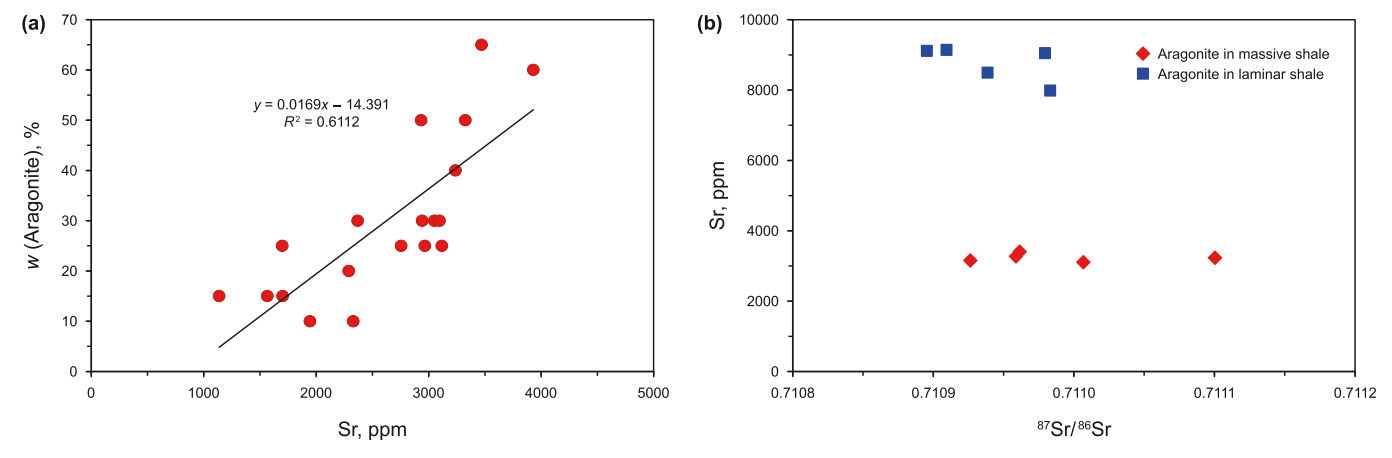


Fig. 6. Sr content and Sr isotope characteristics of aragonite.

Table 3Rare earth element characteristics of aragonite in massive shale (A) and laminar shale (B).

Number	La, ppm	Ce, ppm	Pr, ppm	Nd, ppm	Sm, ppm	Eu, ppm	Gd, ppm	Tb, ppm	Dy, ppm	Ho, ppm	Er, ppm	Tm, ppm	Yb, ppm	Lu, ppm
A1	15.2789	34.6476	3.6322	14.8958	2.7005	0.5051	1.4369	0.2071	1.1640	0.2782	0.8511	0.1186	0.9255	0.1296
A2	16.2850	37.4600	4.1810	17.3044	2.9220	0.4703	1.6824	0.2539	1.7112	0.3760	1.0438	0.1484	1.0653	0.1673
A3	15.5428	34.0737	3.7253	15.9790	2.3359	0.5609	1.7657	0.2472	1.7383	0.2887	1.0367	0.1875	0.9215	0.1372
A4	13.7816	32.8866	3.7126	14.1511	2.7024	0.5704	1.7338	0.2151	1.3623	0.3040	0.8177	0.1288	0.9352	0.0858
A5	15.1159	38.0278	4.1874	16.7884	2.6471	0.5852	2.1930	0.2899	1.9037	0.4299	0.9755	0.1271	1.1845	0.1860
A6	15.3481	35.5194	3.7660	14.5066	2.5473	0.6123	1.9899	0.2711	1.5191	0.3788	0.8941	0.1511	0.8698	0.1359
A7	15.7280	33.7887	3.8081	15.2321	2.4712	0.5931	1.6774	0.3145	1.5528	0.3194	1.0464	0.1472	1.2004	0.1571
A8	15.8834	34.6735	3.9990	15.4505	2.8822	0.4337	1.8853	0.3005	1.6284	0.3188	0.9525	0.1276	0.8484	0.1241
A9	14.4632	32.9152	3.5303	15.3656	2.5425	0.6098	1.7081	0.3226	2.0760	0.3270	1.0840	0.1622	1.0866	0.1809
B1	15.9195	35.3742	4.2424	16.3041	1.6025	0.4380	0.8025	0.0723	0.6638	0.1168	0.4389	0.0721	0.8014	0.1033
B2	16.1053	39.7317	4.1661	18.5902	2.4523	0.4100	1.1111	0.1934	1.1799	0.2349	0.9271	0.1364	0.9109	0.1147
B3	17.5151	39.1271	4.3257	17.2797	2.0623	0.3878	1.1301	0.1558	0.9117	0.2332	0.7258	0.1370	0.9172	0.1409
B4	14.6411	37.4403	4.0819	15.1798	1.9373	0.4857	0.8407	0.1070	0.4843	0.1005	0.2878	0.0433	0.4712	0.0963
B5	12.9535	34.7910	3.3517	14.5736	1.5816	0.3125	0.8748	0.1163	0.6736	0.1598	0.4831	0.0563	0.5736	0.0679
B6	15.8704	37.2540	4.3817	15.1463	1.9812	0.3781	0.8378	0.1172	0.7910	0.1420	0.4483	0.0706	0.7141	0.0769
Average for A	15.2697	34.8881	3.8380	15.5193	2.6390	0.5490	1.7858	0.2691	1.6284	0.3356	0.9669	0.1443	1.0041	0.1449
Average for B	15.5008	37.2864	4.0916	16.1789	1.9362	0.4020	0.9328	0.1270	0.7841	0.1645	0.5518	0.0859	0.7314	0.1000
CI carbonaceous chondrite (McDonough and Sun,1995)	0.2370	0.6130	0.0928	0.4570	0.1480	0.0563	0.1990	0.0361	0.2460	0.0546	0.1600	0.0247	0.1610	0.0246

aragonite are basically the same (Fig. 5(d)). Except for Ga, the content of each trace element in the massive aragonite is much higher than that in the laminar aragonite (Table 4 and Fig. 5(d)).

Regarding the isotopic characteristics, 87 Sr/ 86 Sr generally ranges from 0.710896 to 0.711100 (Fig. 6(b)). The ratio of 87 Sr/ 86 Sr in massive aragonite is slightly higher than that in laminar aragonite (Fig. 6(b)). δ^{13} C of the aragonite is between 5.96 % and 6.36 %, and δ^{18} O is between -6.25 % and -5.74 %, both of which are much higher than that in calcite obtained from the same target interval (Fig. 7).

4. Preservation mechanisms of aragonite

4.1. Favorable diagenetic conditions

Aragonite belongs to the orthorhombic system and theoretically has its own morphology (Pokroy et al., 2006; Oganov et al., 2006; Miyake and Kawano, 2010). However, the morphological characteristics and cathodoluminescence characteristics of aragonite in the shale show that aragonite belongs to biological origin and is composed of algal microbial fossils (Fig. 3(d)-(i)). Regardless of whether it is biogenic or inorganic, existing studies have shown that the thermodynamic stability of aragonite in near-surface environments (syndiagenetic stage) is lower than that of lowmagnesium calcite, leading to the spontaneous transformation of aragonite into low-magnesium calcite (He et al., 2020). During shallow burial, the dissolution of aragonite is mainly caused by aerobic respiration in the oxygen zone, nitrate reduction in the suboxic zone, bacterial sulfide degradation, and methanogenesis in the anoxic zone (Froelich et al., 1979; Berner, 1981; Jørgensen and Kasten, 2006; Su et al., 2020; Munnecke et al., 2023). Additionally, organic matter content (Sanders, 2003; Bradbury and Turchyn, 2019), salinity (Dijkstra et al., 2017), oxygen supply (Munnecke et al., 2023), and the degree of lithification of laminae (Nohl et al., 2020) all indirectly affect the dissolution of aragonite. Our observation further found that shales rich in aragonite develop large amounts of framboidal pyrite (Fig. 3(k)-(l)), suggesting that the bacterial sulfate reduction process is also very active during shallow burial diagenesis. Furthermore, the algal microbial fossils are originally rich in a large amount of organic matter, but why is the aragonite only partially or hardly dissolved (Fig. 3(d))? In fact, the

dissolution, precipitation, and preservation of aragonite during burial are primary related to microbial activity, temperature, pressure, pH, and the ion types and concentrations of diagenetic fluids (Roeser et al., 2016; Facq et al., 2016; Smrzka et al., 2019; Zwicker et al., 2018; Pederson et al., 2020; Guo et al., 2019).

It is evident from several well sections of the rich aragonite shale in the research region that the aragonite content is higher when the burial depth of the aragonite-rich shale is less than 3000 m, particularly when it is less than 2500 m (Fig. 10). In fact, when the burial depth of the Jiyang Depression is less than 2500 m, the R_0 is less than 0.5 % (Fig. 10). This stage belongs to the early diagenetic period, the ground temperature is generally less than 70 °C (Potter et al., 2005; Milliken and Olson, 2017; Milliken et al., 2012, 2021). Therefore, aragonite has not been dissolved because of the low temperature, immature organic materials, and absence of organic acid in the formation.

This viewpoint can be further confirmed by the simulation experiment of aragonite dissolution under high temperature and pressure. The amount of aragonite dissolved rises with the concentration of organic acids (Fig. 8(a)), suggesting that aragonite will dissolve quickly once organic acids are present in the formation. In addition, the Ca²⁺ ion concentration of the aragonite-rich samples in the residual solution of each group of experiments was higher than that of the calcite-rich samples, which shows that aragonite is more likely to dissolve than calcite under the same conditions of temperature, pressure and acid concentration, and further reveals that aragonite would be easily dissolved or transformed to calcite as soon as the organic film (like human teeth) in macroalgal fossils is destroyed (Hall et al., 1967; Rousseau et al., 2005). In sample Y51-2672 m, the algal fossils in the massive area are relatively wellpreserved (Fig. 3(d)), and the internal organic membrane should be intact. Although the fossils in the layered area are somewhat dispersed, they still retain the form of coccoliths (Fig. 3(i)). This suggests that the organic membrane may also not have been damaged, which is conducive to the preservation of aragonite.

It can also be seen from the envelope characteristics of aragonite content in Fig. 10 that when the burial depth is below 2500 m, the aragonite content decreases sharply, and when the burial depth is about 3500 m, the aragonite content is close to 0 wt%. In fact, when the burial depth in the study area is greater than 2500 m, the R_0 also exceeds 0.5 %, and the organic matter enters the mature stage. The

Trace element characteristics of aragonite in massive shale (A) and laminar shale (B)

Li,	ppm Sc, p	ypm V, pp	Li, ppm Sc, ppm V, ppm Cr, ppm		Co, ppm Ni, ppm	Zn, ppm	Ga, ppm	As, ppm I	Rb, ppm	Y, ppm Z	Zr, ppm N	Nb, ppm N	Mo, ppm Cd, ppm Cs, ppm Hf, ppm Ta, ppm Pb, ppm	d, ppm (Cs, ppm	Hf, ppm	Ta, ppm	Pb, ppm	Th, ppm	U, ppm
16	16.573 3.766	36.102	19.021	5.087	17.148	7.835	38.551	4.050	29.376	8.622 1	18.123 3.	3.236 1.	1.437 (2.105	0.479	0.137	7.823	3.854	1.375
19	19.189 5.036	16 48.796	36 24.407	9.337	38.803	7.800	33.269	12.408	37.895	9.981 2	28.589 3.	3.424 3.	Ī		2.647	0.762	0.268		4.836	1.765
20	20.076 3.894	45.484	34 27.364	5.310	8.242	7.605	37.222	. ,	39.504	8.983 2		_	0.814 (0.024	3.057	0.557	0.175	4.169	3.944	1.345
24	24.372 4.941	11 53.335	35 29.201	5.445	9.738	10.011	33.763	2.050	44.528 8	8.682 2	22.714 2.	_	Ū	. ,	3.211	0.774	0.169	4.303	3.963	1.268
24	24.653 4.213	3 43.413	13 24.817	2.606	8.202	10.437	37.828	5.959		11.561 1	19.275 2.		_		2.828	0.540	0.193	11.722	5.127	1.715
21	21.272 4.506	16 43.074	74 23.800	4.680	24.271	31.799	33.051	5.536	38.692	9.819 2					2.912	0.850	0.189	10.946	4.130	1.489
21	21.987 4.451	1 45.556	56 24.592	6.795	24.999	8.532	32.704	9.457	38.664	9.713 2	29.738 5.	• ,	_		2.995	0.574	0.389	21.294	4.704	2.563
21	21.852 4.817		07 24.126	8.026	32.501	7.365	33.125	4		9.590 2			_	•	2.703	0.717	0.172	19.945	4.073	1.486
18	18.649 4.400	00 40.096	96 23.015	10.622	49.160	8.450	34.802	13.544	38.287	ω.				•	2.523	0.622	0.159	25.588	4.274	1.563
4.5	4.585 0.544	4 3.235	5 1.000	0.125	1.436	0.704	66.185	0.263	0.354	4.638 0	0.603 0.	0.136 0.	0.074	000.0	0.056	0.022	600.0	0.491	0.661	0.639
4.5	4.525 0.403	3 2.285	5 0.280	3.349	9.784	1.019	77.522	3.642 (0.408	8.247 0	0.739 0.	0.069 1.	_	.132 (0.061	0.001	0.003	12.779	1.304	0.702
4.4	4.409 0.970	'0 2.640	00000 0	1.101	3.208	0.814	78.053	1.400 (_		_).181 (Ū	0.022	0.014	0.000	0.938	1.455	0.611
3.5	3.908 0.200	0 2.874	1.046	0.180	1.790	0.782	64.069	0.447 (0.226	3.541 0	0.582 0.	0.023 0.	0.119	0.000	0.015	0.016	0.000	0.912	0.737	0.701
4.8	4.892 0.301	11 4.139	00000 6	0.126	1.177	0.644	67.304	0.484 (6.117 0		Ū		Ū	0.028	800.0	0.001	0.440	1.030	0.586
4.4	4.494 0.606	06 2.400) 2.347	0.049	1.843	0.163	72.743	0.581 (0.550	2.997 0	0.634 0.	0.091 0.	0.146 (0000	0.065	0.014	0.000	0.485	1.004	989.0
Average for A 20.958	.958 4.447	17 44.252	52 24.483	6.434	23.674	11.093	34.924	7.409	38.478	9.762 2	24.673 2.	2.915 2.	2.703	0.122	2.776	0.653	0.206	14.158	4.323	1.619
Average for B 4.469	169 0.504	2.929	9 0.779	0.822	3.206	0.688	70.980	1.136 (0.501	6.300 0	0.644 0.	0.065 0.	0.281 (0.025	0.041	0.013	0.002	2.674	1.032	0.654
1.5	.500 5.920		0 2650.0C)0 500.00C	56.000 2650.000 500.000 10500.000 31	0.000	9.200	1.850	2.300	1.570 3	3.820 0.	0.240 0.	0.900	0.710	0.190	0.103	0.014	2.470	0.029	0.007
of CI (CI ca	rbonaceou	s chondrit	e) derived f	from McDo	The data of CI (CI carbonaceous chondrite) derived from McDonough and Suna	ına (1995).														

Aragonite in laminar shale

Micritic calcite

Aragonite in massive shale

Aragonite in massive shale

Sparry calcite

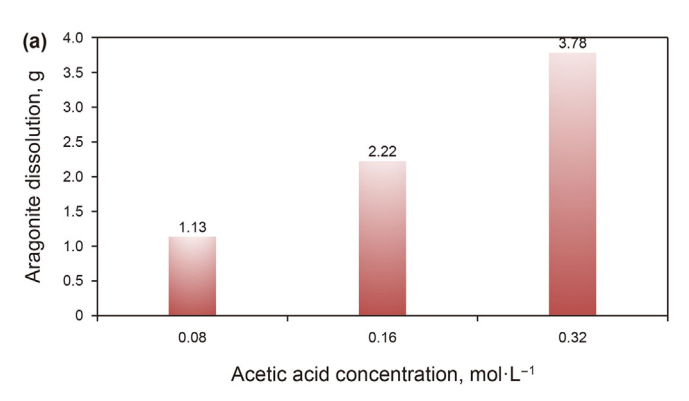
Fig. 7. Micro-area carbon-oxygen isotopic characteristics of aragonite and calcite.

presence of organic acids leads to the dissolution of aragonite, resulting in a decrease in the content. In addition, the increase of temperature also aggravated the damage to the organic film wrapped around aragonite, further promoting the dissolution of aragonite by organic acid. When the burial depth reaches 3500 m, the R_0 is close to 0.8 %, the organic matter enters the peak period of hydrocarbon generation, and a large amount of organic acid is released, so the aragonite is dissolved and disappeared. In view of the above, low temperature and lack of organic acid are important reasons for the preservation of aragonite in shale during diagenesis. In addition, the calcite content shows a significant upward trend after entering the hydrocarbon generation threshold (Fig. 10), which further illustrates the transformation of aragonite to calcite in a relatively closed shale diagenetic system is an important source of increased calcite content. Of course, the clay minerals in the study area are mainly composed of I/S mixed layer and illite (Fig. 10). A large amount of calcium ions is also released during the illiteization of smectite, which is also an important mechanism for the increase of calcite content (Boles and Stephen, 1979; Bethke and Altaner, 1986; Rask et al., 1997; Robinson et al., 2002; Beaufort et al., 2015; Xiong et al., 2022).

Furthermore, there might be additional factors influencing aragonite preservation. Shale is characterized by tiny pores, low porosity, poor permeability, and tight texture. Additionally, each shale strata sequence (e.g., Es1, Es3 and Es4) exhibits considerable thickness (with a maximum exceeding 1 km) (Liu and Xia, 2007). This creates challenges for external diagenetic fluids to penetrate the pore system of shale (Jarvie, 2012), thereby allowing aragonite to be preserved.

4.2. Favorable sedimentary conditions

The deposition of aragonite is closely related to the ion composition, ion concentration, temperature, and pH of the water (Ben Dor et al., 2021; Ma et al., 2017; Wassenburg et al., 2012; Shiraishi et al., 2020; Christensen et al., 2021). Previous studies have shown that higher salinity, Mg/Ca ratio, and pH are favorable for the deposition and preservation of aragonite (Wassenburg et al., 2012; Ma et al., 2017; Shiraishi et al., 2020). From the geochemical characteristics of the research area (Fig. 10), during the periods from upper Es4, lower Es3 to Es1 of the Shahejie Formation, although there are differences in the paleoclimatic environments of each period, these periods generally exhibit a warm and humid climate (Mg/Ca ratio ranging from 0 to 1 indicating a humid climate, as shown in Fig. 10) (Liu and Zhou, 2007; Shi et al., 2018,



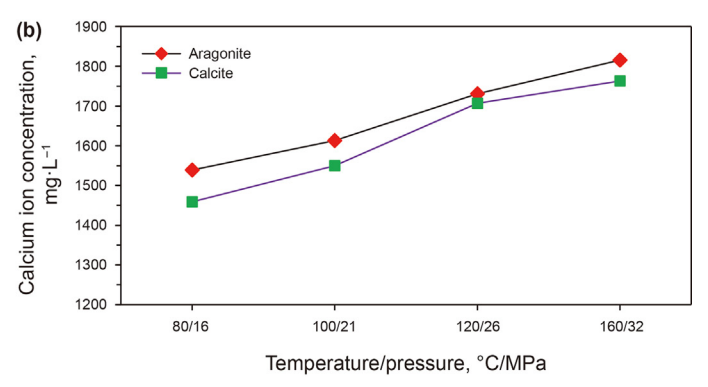


Fig. 8. Simulation experiment on the dissolution of aragonite under high temperature and pressure. (a) The relationship between organic acid concentration and aragonite dissolution. (b) The concentration of calcium ions released from the simulation experiments of aragonite and calcite dissolution under different temperature and pressure conditions.

2020, 2021), and the water is alkaline (Zhu et al., 2022), which is very conducive to the development of aragonite. Especially during warm climatic periods, algae flourish, laying the foundation for the abundant production of biogenic aragonite (Warren, 2010). While Mg is readily integrated into the calcite crystal lattice, it is not as easily incorporated into the aragonite crystal lattice (Melim et al., 2002; Swart, 2015). High Mg/Ca ratios and low supersaturation thus have no effect on the rate of precipitation of aragonite, but they significantly decrease or prevent the precipitation of calcite (De Choudens-Sánchez and González, 2009). During the periods from upper Es4, lower Es3 to Es1 of the Shahejie Formation, although there are differences in the water salinity and Mg/Ca ratio between different periods, these periods generally exhibit higher salinity (Sr/Ba greater than 1 indicating a saline environment, as shown in Fig. 10) (Liu and Zhou, 2007; Peng et al., 2021) and higher Mg/Ca ratios (Khan et al., 2023) in the sedimentary environment, which provides necessary conditions for the precipitation of

Furthermore, deep water condition and hypoxic environment are important factors for the preservation of algal organisms after deposition, thereby promoting the non-dissolution or nontransformation of calcite (Kelts, 1988; Makeen et al., 2015). The Fe/Mn ratio reflects the ancient water depth, with Fe typically depositing in nearshore environments; a high Fe content indicates relatively shallow water. In contrast, the more stable Mn element has a slower deposition rate and can migrate over long distances to basins far from the shore, meaning that a higher Mn content signifies greater water depth during sediment deposition (Chen et al., 2008). An Fe/Mn ratio greater than 100 is considered to indicate a shallow lake environment, a ratio of 60-100 indicates a semi-deep lake, and a ratio less than 60 indicates a deep lake environment (Wang et al., 2013). From Fig. 9(a), it can be observed that the Fe/Mn values in the aragonite-rich massive and laminated shales are generally less than 60, especially the Fe/Mn ratio in the aragoniterich massive shale is lower, only about 20, indicating that the sedimentary environment of rich algal shale belongs to a deep lake environment. Additionally, (Fe + Al)/(Ca + Mg) is also an important indicator for reflecting the depth of the water. Both Fe and Al have higher concentrations in terrestrial clastic rocks, decreasing in mudstones as carbonate minerals accumulate, while Ca and Mg are primarily associated with carbonate rocks (Zhang et al., 2003). The (Fe + Al)/(Ca + Mg) ratio greater than 1 corresponds to a shallow lake environment, a ratio of 1-0.5 indicates a semi-deep lake environment, and a ratio less than 0.5 represents to a deep lake environment (Wang et al., 2013). From a statistical analysis (Fig. 9(A)), (Fe + Al)/(Ca + Mg) ratio in the aragonite-rich massive and laminated shales less than 0.5 further confirms that the sedimentation of rich algal shale occurred in a deep lake environment.

V/(V + Ni) and Ni/Co have been widely used to indicate the degree of oxidation-reduction in ancient lake waters (Jones and Manning, 1994). Strong reducing environments, such sulfidic conditions, can cause V to precipitate as V(OH)3 or V2O3, or it can change into a +3 valence state and be absorbed by nearby porphyrins (Wanty and Goldhaber, 1992). Ni penetrates the pyrite crystal lattice as insoluble NiS in strong reducing conditions, where it fixes itself in sediments (Morse and Luther Iii, 1999). In reducing sedimentary conditions, nickel (Ni) can occasionally infiltrate sediments with organic matter and be stored as Ni-porphyrins (Grosjean et al., 2004). Ni's migratory capacity declines more quickly in stronger reducing environments than in Co., which makes it more susceptible to adsorption and deposition (Chang et al., 2009). Sedimentary habitats with V/(V + Ni) > 0.54 imply anaerobic conditions, those with 0.45-0.60 indicate suboxic conditions, while those with <0.45 indicate oxygen-rich conditions. Generally, a Ni/Co ratio greater than 1.8 suggests a reducing environment. The analysis indicates that V/(V + Ni) values in the aragonite-rich massive and laminated shales are generally greater than 5 (Fig. 9(b)). Ni/Co values in the aragonite-rich massive and laminated shales mostly range from 2 to 10, with a maximum value of 39 (Fig. 9(b)), indicating a relatively strong reducing nature of the water during aragonite-rich shale deposition.

5. Geological significance

5.1. Indicating specific sedimentary environment

Most of these aragonites are dominated by algal microbial fossils, especially coccolithophores. In general, coccolithophores belong to marine organisms (Aksu et al., 2002; Steiner et al., 2019), but the target formation in the study area belongs to terrestrial basins, so why do marine organisms to be produced?

This question is further resolved by the analysis of geochemical indicators. The Sr/Ba ratio is an important indicator to determine paleosalinity. Strontium has a stronger migration ability than barium. In freshwater lake, the water medium is relatively acidic, the salinity is very low, and the sulfate ion content is low, so both strontium and barium are retained with the form of bicarbonate in the lake water. When the lake water becomes salty and the salinity increases, the barium is first precipitated in the form of barium sulfate, while the strontium is only precipitated when the lake water or seawater is concentrated to a certain extent. It is generally believed that the Sr/Ba ratio of salty (marine) water media is greater

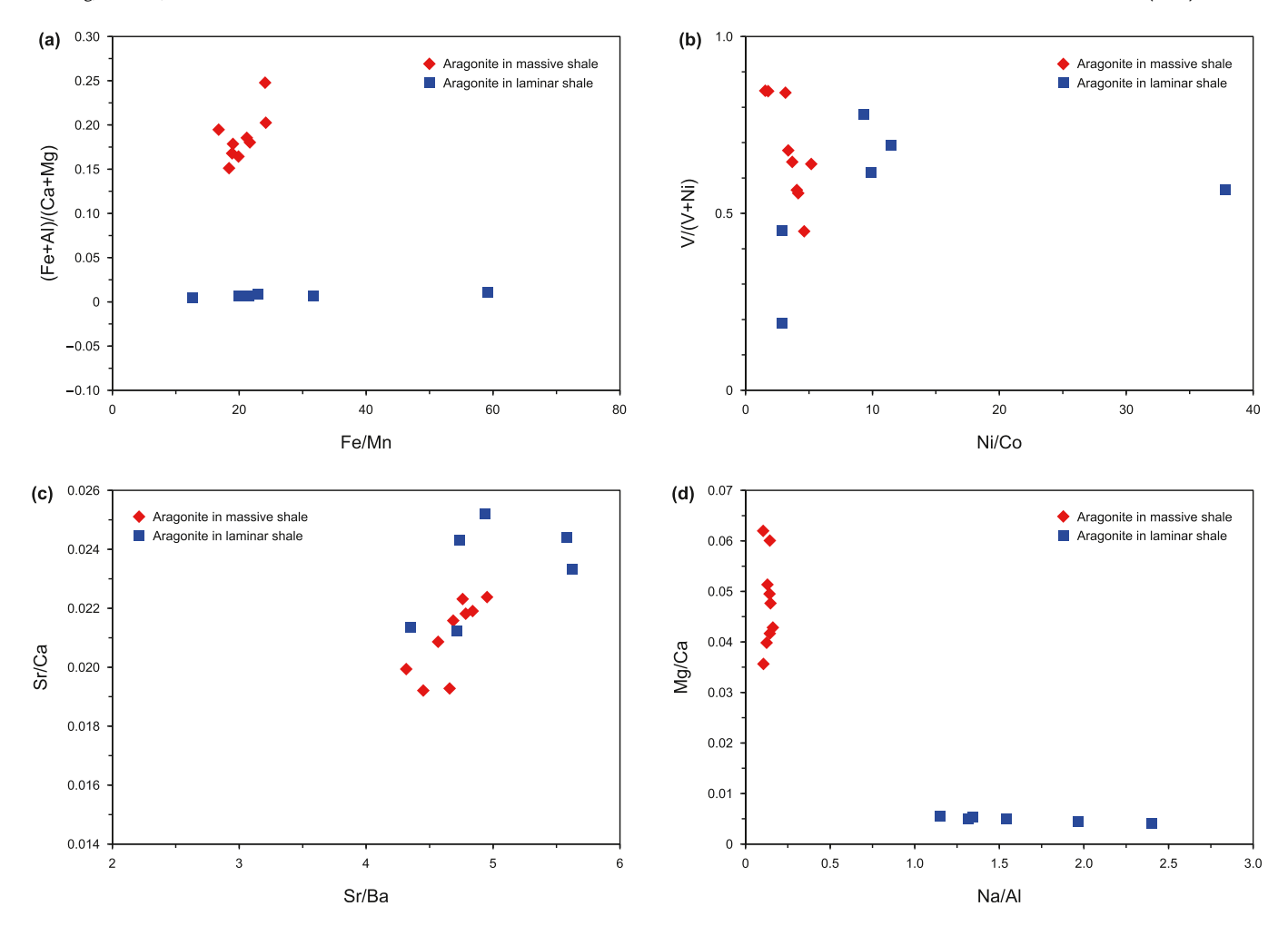


Fig. 9. Characteristics of paleoenvironmental parameters of aragonite-rich shale deposits.

than 1, while the Sr/Ba ratio of freshwater media is less than 1 (Song, 2005; Chen et al., 2008; Wang et al., 2020). The analysis shows that the Sr/Ba ratio the aragonite-rich massive and laminated shales is between 4 and 6 (Fig. 9(c)), indicating that the sedimentary environment is saline (Marine) water medium. In addition, the Z value calculated by combining carbon and oxygen isotope values is also an important indicator to judge the marine and continental sedimentary environment (Keith and Weber, 1964), as shown in Eq. (1).

$$Z = a \left(\delta^{13}C + 50 \right) + b \left(\delta^{18}O + 50 \right) \tag{1}$$

The values of parameters a and b are 2.048 and 0.898, respectively. Generally, a Z value greater than 120 is a marine environment, and less than 120 is a terrestrial environment (Keith and Weber, 1964). From the micro-area carbon and oxygen isotopic values of the shale aragonite, the average value of δ^{13} C is about 6 ‰, and the average value of δ^{18} O is about -6 ‰ (Fig. 7), so the Z value is calculated to be about 136, which further indicates that the depositional environment of aragonite is seawater environment.

In summary, the depositional environment of these aragonites should belong to an abnormal terrestrial environment, i.e., in the case of a terrestrial environment, the basin communicated with seawater intermittently, and some wide salinity plankton invaded the lake. In addition, ⁸⁷Sr/⁸⁷Sr, carbon and oxygen isotope values, and some element contents or ratios are important indicators of paleoclimate (Marais et al., 1992; Song, 2005; Song et al., 2007;

Fruchter et al., 2016; Hermoso et al., 2016; Jia et al., 2017; Phan et al., 2018). For example, the ⁸⁷Sr/⁸⁶Sr value in the aragonite is relatively high (ranging from 0.710896 to 0.711100), while the average value of ⁸⁷Sr/⁸⁶Sr in the shale series of the Jiyang Depression is only about 0.710492 (Liu, 2019); The ratios of Na/Al and Mg/Ca are large (Fig. 9(d)), all of which indicate that the environment at that time was a warm and humid climate to allow the survival and reproduction of these invading plankton, resulting in the mixing of marine organisms in the lacustrine biota species, which has also been confirmed in previous studies (Zhong et al., 1988; Liu and Xu, 2000; 2001; Gong et al., 2019).

5.2. Source and storage space of shale oil

The importance of planktonic algae to lacustrine shale oil generation has been widely recognized (Wu et al., 1998; Liu and Xu, 2000; Wang et al., 2017a). It can be observed from the scanning electron microscope images that the coccolithophores are rich in large amounts of organic matter (Fig. 3(d)–(f)). When the burial depth reaches the hydrocarbon generation threshold, the thermal evolution of these organic matters is the direct source of shale oil. Wu et al. (1998) conducted a thermal simulation hydrocarbon generation experiment on *Emiliania huxleyi* of modern coccolithophores, and the results showed that the amount of "chloroform pitch A", saturated hydrocarbons and aromatic hydrocarbons produced by pyrolysis at 300 °C was the highest, and the saturated hydrocarbon yield reach 2.8% of the dry cell weight, which was

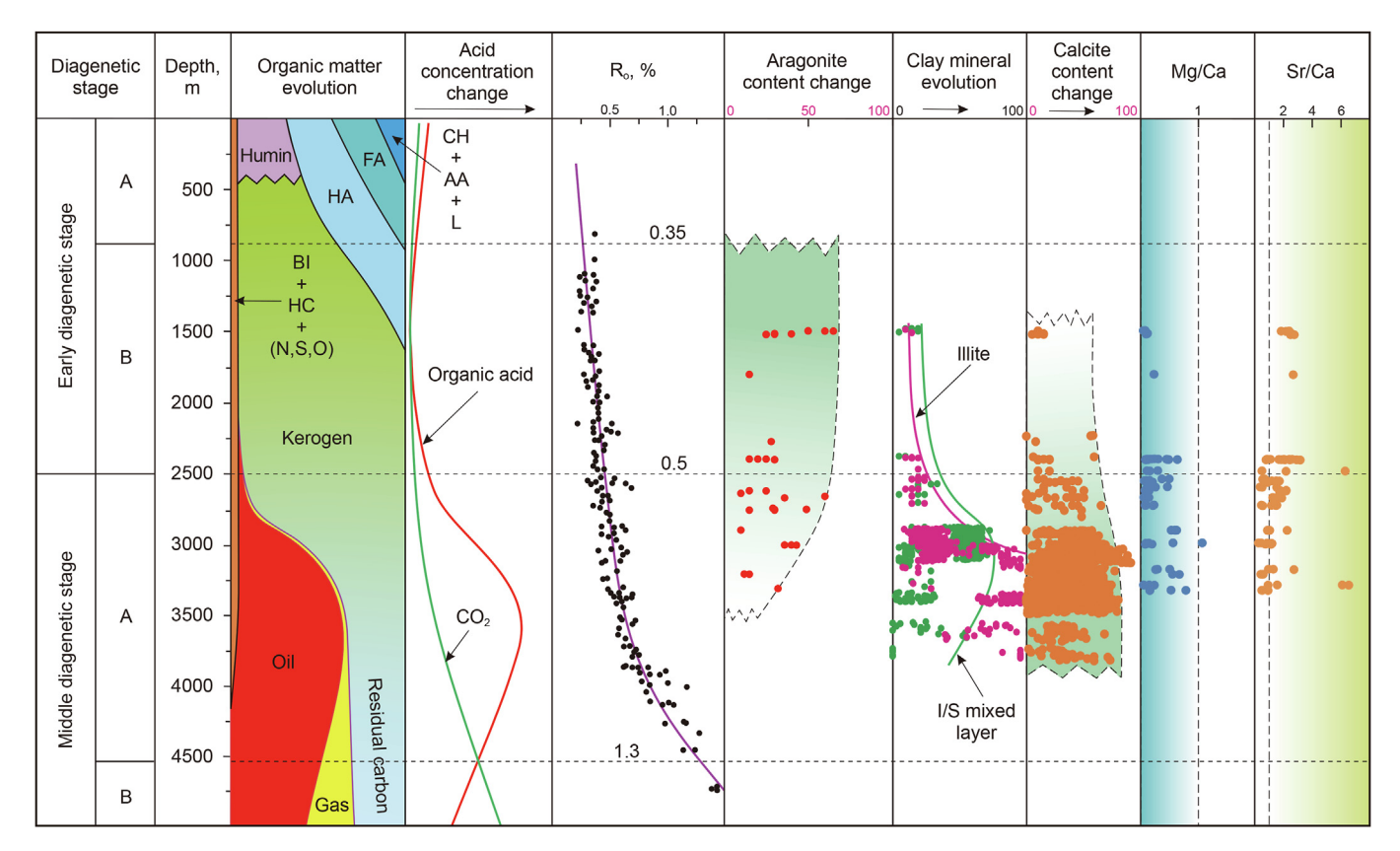


Fig. 10. Diagenetic evolution characteristics of the Paleogene shale aragonite in the Jiyang Depression. Note: Thermal evolution characteristics of organic matter were modified from Tissot et al. (1974); Acid concentration changes was modified from Xiong et al. (2024). R_0 —Vitrinite reflectance; BI + HC + N, S, O—Inherited bitumen + hydrocarbons + nitrogen, sulfur and oxygen compounds; HA—Humic acid; FA—Fulphic acid; CH—Carbohydrates; AA— Amino acid; L—lipid.

6–15 times that of other algae. In addition, Liu and Xu (2000) considered coccolithophores to be the direct source of low-mature oils, which are generally rich in phytane and gammacerane.

In carbonate-rich shale, laminated sparry calcite with intercrystalline pores is the most important storage space for shale oil (Liu et al., 2019), with maximum pore sizes reaching up to 100 µm (Shi et al., 2022). Studies have shown that these laminar sparry calcite crystals are mainly recrystallized from micritic calcite under the action of organic acids, often containing a large amount of impurity minerals such as microcrystalline quartz, albite, and dolomite (Liang et al., 2018; Xiong et al., 2024). In fact, a large portion of this micritic calcite is initially transformed from metastable aragonite (Steinen, 1982; Munnecke et al., 2023). Particularly, biogenic aragonite gradually transforms into micritic and sparry calcite during burial diagenesis, with crystal size increasing and intercrystalline pores enlarging (Hashim and Kaczmarek, 2021; Munnecke et al., 2023). Furthermore, studies have found that these aragonite laminations are interlayered with organic-rich clay laminations. As the maturity stage is reached, the organic matter in the clay laminations generates a significant amount of hydrocarbons and organic acids. The clay minerals, mainly montmorillonite, transform into lamellar illite-smectite mixed layers, releasing a significant quantity of interlayer and structural water (Soto et al., 2021). Under the coupled effects of hydrocarbon generation and dehydration pressure, liquid hydrocarbons, organic acids, and other evolution products in the organic-rich clay laminations migrate towards the larger pores in the carbonate laminations through intercrystalline in the clay minerals and bedding-plane fractures (Xiong et al., 2022). Meanwhile, the aragonite in the carbonate laminations further undergoes dissolution or transformation into calcite due to the action of organic acids, and the continuously recrystallized calcite transforms into coarser crystals, accelerating the shale oil enrichment and storage (Xiong et al., 2022; Wang et al., 2017b).

6. Conclusions

- Aragonite in the Paleogene shale of the Jiyang Depression is related to algal microbial fossils, especially characterized by coccoliths.
- (2) The primary factor allowing biological aragonite to be preserved is the immaturity of the organic matter and the deficiency of abundant organic acids necessary for its dissolution or transformation. Additional factors that may aid in the preservation of aragonite are the ideal sedimentation conditions, the defense of organic coating, and the enclosed environment with tiny pores, low porosity, and low permeability.
- (3) The aragonite-rich shales, characterized by coccolithophores, provide a solid evidence for seawater intrusion into terrestrial lake basin, and have a significant implication for the source and storage of shale oil.

CRediT authorship contribution statement

Zhou-Hai Xiong: Writing — original draft, Methodology, Funding acquisition, Formal analysis. **Ying-Chang Cao:** Writing — review

& editing, Supervision. **Song Xue:** Formal analysis. **Guan-Min Wang:** Writing — review & editing, Supervision. **Chao Liang:** Writing — review & editing. **Ke-Yu Liu:** Writing — review & editing, Investigation.

Declaration of competing interest

The data involved in the manuscript has no conflict of interest and has been authorized by all authors listed. The work described was original research that has not been published previously, and not under consideration for publication elsewhere.

Acknowledgments

This study was supported by the National Natural Science Foundation of China (Nos. 42302152, 42072164, 41821002, and 42272119), the Natural Science Foundation of Shandong Province (No. ZR2023QD076), the Shandong Provincial Key research and Development Program (No. 2020ZLYS08), the Taishan Scholars Program (No. TSQN201812030), and the Fundamental Research Funds for the Central Universities (No. 22CX06010A), Qingdao Postdoctoral Application Research Project (No. QDBSH20220202075). The authors express their sincere gratitude to them.

Appendix A. Supplementary data

Supplementary data to this article can be found online at https://doi.org/10.1016/j.petsci.2024.05.019.

References

- Aksu, A.E., Hiscott, R.N., Kaminski, M.A., Mudie, P.J., Gillespie, H., Abrajano, T., Yaşar, D., 2002. Last glacial—Holocene paleoceanography of the Black Sea and Marmara Sea stable isotopic, foraminiferal and coccolith evidence. Mar. Geol. 190, 119–149. https://doi.org/10.1016/S0025-3227(02)00345-6.
- Balthasar, U., Cusack, M., 2015. Aragonite-calcite seas—quantifying the gray area. Geology 43, 99–102. https://doi.org/10.1130/G36293.1.
- Beaufort, D., Rigault, C., Billon, S., Billault, V., Inoue, A., Inoue, S., Patrier, P., 2015. Chlorite and chloritization processes through mixed-layer mineral series in low-temperature geological systems-a review. Clay Miner. 50, 497–523. https://doi.org/10.1180/claymin.2015.050.4.06.
- Ben Dor, Y., Flax, T., Levitan, I., Enzel, Y., Brauer, A., Erel, Y., 2021. The paleohydrological implications of aragonite precipitation under contrasting climates in the endorheic Dead Sea and its precursors revealed by experimental investigations. Chem. Geol. 576, 120261. https://doi.org/10.1016/j.chemgeo.2021.120261.
- Berner, R.A., 1981. A new geochemical classification of sedimentary environments.

 J. Sediment. Res. 51, 359–365. https://doi.org/10.1306/212F7C7F-2B24-11D7-8648000102C1865D
- Bethke, C.M., Altaner, S.P., 1986. Layer-by-layer mechanism of smectite illitization and application to a new rate law. Clay Clay Miner. 34, 136–145. https://doi.org/10.1346/ccmn.1986.0340204.
- Boles, J.R., Stephen, G.F., 1979. Clay diagenesis in Wilcox sandstones of southwest Texas implications of smectite diagenesis on sandstone cementation. SEPM J. Sediment. Res. 49. https://doi.org/10.1306/212F76BC-2B24-11D7-8648000102C1865D, 0055-0070.
- Bots, P., Benning, L.G., Rickaby, R.E.M., Shaw, S., 2011. The role of SO_4 in the switch from calcite to aragonite seas. Geology 39, 331–334. https://doi.org/10.1130/G31619.1.
- Bottrell, S., Raiswell, R., 1989. Primary versus diagenetic origin of Blue Lias rhythms (Dorset, UK): evidence from sulphur geochemistry. Terra. Nova 1, 451–456. https://doi.org/10.1111/j.1365-3121.1989.tb00409.x.
- Brachert, T.C., Dullo, W.C., 2000. Shallow burial diagenesis of skeletal carbonates selective loss of aragonite shell material (Miocene to Recent, Queensland Plateau and Queensland Trough, NE Australia). Sediment. Geol. 136, 169–187. https://doi.org/10.1016/S0037-0738(00)00096-8.
- Bradbury, H.J., Turchyn, A.V., 2019. Reevaluating the carbon sink due to sedimentary carbonate formation in modern marine sediments. Earth Planet Sci. Lett. 519, 40–49. https://doi.org/10.1016/j.epsl.2019.04.044.
- Burdige, D.J., Hu, X., Zimmerman, R.C., 2010. The widespread occurrence of coupled carbonate dissolution/reprecipitation in surface sediments on the Bahamas Bank. Am. J. Sci. 310, 492–521. https://doi.org/10.2475/06.2010.03.
- Burton, E.A., Walter, L.M., 1987. Relative precipitation rates of aragonite and Mg calcite from seawater: temperature or carbonate ion control? Geology 15, 111–114. https://doi.org/10.1130/0091-7613(1987)15<111:RPROAA>2.0.CO;2.

Chang, H.J., Chu, X.L., Feng, L.J., Huang, J., 2009. Redox sensitive trace elements as paleoenvironments proxies. Geol. Rev. 55, 91–99. https://doi.org/10.16509/j.georeview.2009.01.014 (in Chinese).

- Chen, Z.H., Cha, M., Jin, Q., 2008. Mineral elemental response to the evolution of terrestrial brine faulted-basin:a case study in the Paleogene of Well Haoke-1. Acta Sedimentol. Sin. 26, 925–932. https://doi.org/10.14027/ j.cnki.cjxb.2008.06.015 (in Chinese).
- Chen, Z.H., Huang, W., Liu, Q., Zhang, L.Y., Zhang, S.C., 2016. Geochemical characteristics of the paleogene shales in the dongying depression, eastern China. Mar. Petrol. Geol. 73, 249–270. https://doi.org/10.1016/j.marpetgeo.2016.02.022.
- Christensen, J.N., Watkins, J.M., Devriendt, L.S., DePaolo, D.J., Conrad, M.E., Voltolini, M., Yang, W., Dong, W., 2021. Isotopic fractionation accompanying CO₂ hydroxylation and carbonate precipitation from high pH waters at the Cedars, California, USA. Geochem. Cosmochim. Acta 301, 91–115. https://doi.org/10.1016/j.gca.2021.01.003.
- Cuif, J.P., Dauphin, Y., Meibom, A., Rollion-Bard, C., Salomé, M., Susini, J., Williams, C.T., 2008. Fine-scale growth patterns in coral skeletons: biochemical control over crystallization of aragonite fibres and assessment of early diagenesis. Geol. Soc., London, Spec. Publ. 303, 87–96. https://doi.org/10.1144/SP303.7.
- De Choudens-Sanchez, V., Gonzalez, L.A., 2009. Calcite and aragonite precipitation under controlled instantaneous supersaturation: elucidating the role of CaCO₃ saturation state and Mg/Ca ratio on calcium carbonate polymorphism. J. Sediment. Res. 79, 363–376. https://doi.org/10.2110/jsr.2009.043.
- Dijkstra, N., Quintana Krupinski, N.B., Yamane, M., Obrochta, S.P., Miyairi, Y., Yokoyama, Y., Slomp, C.P., 2017. Holocene refreshening and reoxygenation of a bothnian sea estuary led to enhanced phosphorus burial. Estuar. Coast 41, 139–157. https://doi.org/10.1007/s12237-017-0262-x.
- Dix, G.R., Nelson, C.S., 2006. Diagenetic potential for lithification of cool-water carbonate shelf mud. Sediment. Geol. 185, 41–58. https://doi.org/10.1016/ i.sedgeo.2005.10.003.
- Drupp, P.S., De Carlo, E.H., Mackenzie, F.T., 2016. Porewater CO₂—carbonic acid system chemistry in permeable carbonate reef sands. Mar. Chem. 185, 48–64. https://doi.org/10.1016/j.marchem.2016.04.004.
- Facq, S., Daniel, I., Montagnac, G., Cardon, H., Sverjensky, D.A., 2016. Carbon speciation in saline solutions in equilibrium with aragonite at high pressure. Chem. Geol. 431, 44–53. https://doi.org/10.1016/j.chemgeo.2016.03.021.
- Froelich, P.N., Klinkhammer, G., Bender, M.L., Luedtke, N., Heath, G.R., Cullen, D., Dauphin, P., Hammond, D., Hartman, B., Maynard, V., 1979. Early oxidation of organic matter in pelagic sediments of the eastern equatorial Atlantic: suboxic diagenesis. Geochem. Cosmochim. Acta 43, 1075—1090. https://doi.org/10.1016/0016-7037/79)90095-4.
- Fruchter, N., Eisenhauer, A., Dietzel, M., Fietzke, J., Böhm, F., Montagna, P., Stein, M., Lazar, B., Rodolfo-Metalpa, R., Erez, J., 2016. ⁸⁸Sr/⁸⁶Sr fractionation in inorganic aragonite and in corals. Geochem. Cosmochim. Acta 178, 268–280. https://doi.org/10.1016/j.gca.2016.01.039.
- Gao, J.F., Zhou, M.F., 2013. Generation and evolution of siliceous high magnesium basaltic magmas in the formation of the Permian Huangshandong intrusion (Xinjiang, NW China). Lithos 162, 128–139. https://doi.org/10.1016/ i.lithos.2013.01.002.
- Gong, B.H., Sun, Y.T., Liu, J., Li, H., 2019. Origin analysis of high-quality source rocks in the lower Es1 of Zhanhua Sag, Jiyang Depression. Geol. Rev. 65, 632–644. https://doi.org/10.16509/j.georeview.2019.03.009.
- Grosjean, E., Adam, P., Connan, J., Albrecht, P., 2004. Effects of weathering on nickel and vanadyl porphyrins of a Lower Toarcian shale of the Paris basin. Geochem. Cosmochim. Acta 68, 789–804. https://doi.org/10.1016/S0016-7037(03)00496-4
- Guo, Y.R., Deng, W.F., Wei, G.J., 2019. Kinetic effects during the experimental transition of aragonite to calcite in aqueous solution: insights from clumped and oxygen isotope signatures. Geochem. Cosmochim. Acta 248, 210–230. https://doi.org/10.1016/j.gca.2019.01.012.
- Gussone, N., Böhm, F., Eisenhauer, A., Dietzel, M., Heuser, A., Teichert, B.M.A., Reitner, J., Wörheide, G., Dullo, W.C., 2005. Calcium isotope fractionation in calcite and aragonite. Geochem. Cosmochim. Acta 69, 4485–4494. https://doi.org/10.1016/j.gca.2005.06.003.
- Hall, A., Kennedy, W., Taylor, J.H., 1967. Aragonite in fossils. Proc. R. Soc. B. Biol. Sci. 168, 377–412. https://doi.org/10.1098/rspb.1967.0071.
- Hashim, M.S., Kaczmarek, S.E., 2021. The transformation of aragonite to calcite in the presence of magnesium: implications for marine diagenesis. Earth Planet Sci. Lett. 574. https://doi.org/10.1016/j.epsl.2021.117166.
- He, M., Cai, Y.J., Zhang, H.W., Xue, G., Cheng, X., Lu, Y.B., Wang, G.Z., Qin, X.L., Ma, L., Wei, Y., Huang, S.Y., Chang, H., Yan, H., 2021. The impact and implications of aragonite-to-calcite transformation on speleothem trace element composition. Sediment. Geol. 425, 106010. https://doi.org/10.1016/j.sedgeo.2021.106010.
- He, R., Ning, M., Huang, K.J., Ma, H.R., Shen, B., 2020. Mg isotopic systematics during early diagenetic aragonite-calcite transition: insights from the Key Largo Limestone. Chem. Geol. 558. https://doi.org/10.1016/j.chemgeo.2020.119876.
 Hermoso, M., Minoletti, F., Aloisi, G., Bonifacie, M., McClelland, H.L.O.,
- Hermoso, M., Minoletti, F., Aloisi, G., Bonifacie, M., McClelland, H.L.O., Labourdette, N., Renforth, P., Chaduteau, C., Rickaby, R.E.M., 2016. An explanation for the ¹⁸O excess in Noelaerhabdaceae coccolith calcite. Geochem. Cosmochim. Acta 189, 132–142. https://doi.org/10.1016/j.gca.2016.06.016.
- Higgins, J.A., Blättler, C.L., Lundstrom, E.A., Santiago-Ramos, D.P., Akhtar, A.A., Crüger Ahm, A.S., Bialik, O., Holmden, C., Bradbury, H., Murray, S.T., Swart, P.K., 2018. Mineralogy, early marine diagenesis, and the chemistry of shallow-water carbonate sediments. Geochem. Cosmochim. Acta 220, 512–534. https://doi.org/

10.1016/j.gca.2017.09.046.

- Hodell, D.A., Mead, G.A., Mueller, P.A., 1990. Variation in the strontium isotopic composition of seawater (8 Ma to present): implications for chemical weathering rates and dissolved fluxes to the oceans. Chem. Geol. Isot. Geosci. 80, 291–307. https://doi.org/10.1016/0168-9622(90)90011-Z.
- James, N.P., Bone, Y., Kyser, T.K., 2005. Where has all the aragonite gone? Mineralogy of Holocene Neritic cool-water carbonates, Southern Australia. J. Sediment. Res. 75, 454–463. https://doi.org/10.2110/jsr.2005.035.
- James, N.P., Narbonne, G.M., Armstrong, A.K.R., Betzler, C., 2020. Aragonite depositional facies in a late ordovician calcite sea, eastern laurentia. Sedimentology 67, 3513–3532. https://doi.org/10.1111/sed.12753.
- Jarvie, D.M., 2012. Shale resource systems for oil and gas: Part 2—shale-gas resource systems. In: Breye, J.A. (Ed.), Shale Reservoirs—Giant Resources for the 21st Century. AAPG Memoir, pp. 69–87. https://doi.org/10.1306/13321447M973489.
- Jia, P., Li, W., Lu, Y.Z., Fan, R., Li, X., Yuan, F., Chen, Y.H., Li, M., Zeng, Y.Y., Liu, X., 2017. The carbon and oxygen isotopic compositions and their evolution of the Xixiangchi Group carbonate rocks in Sichuan Basin and their geological implications. J. Radioanal. Nucl. Chem. 311, 755–768. https://doi.org/10.1007/s10967-016-5102-0.
- Jones, B., 2017. Review of aragonite and calcite crystal morphogenesis in thermal spring systems. Sediment. Geol. 354, 9–23. https://doi.org/10.1016/ j.sedgeo.2017.03.012.
- Jones, B., Manning, D.A., 1994. Comparison of geochemical indices used for the interpretation of palaeoredox conditions in ancient mudstones. Chem. Geol. 111, 111–129. https://doi.org/10.1016/0009-2541(94)90085-X.
- Jørgensen, B.B., Kasten, S., 2006. Sulfur cycling and methane oxidation. Mar. geochem. 271–309. https://doi.org/10.1007/3-540-32144-6_8.
- Keith, M.L., Weber, J.N., 1964. Carbon and oxygen isotopic composition of selected limestones and fossils. Geochem. Cosmochim. Acta 28, 1787–1816. https:// doi.org/10.1016/0016-7037(64)90022-5.
- Kelts, K., 1988. Environments of Deposition of Lacustrine Petroleum Source Rocks: an Introduction, vol. 40. Spec. Publ., Geol. Soc., London, pp. 3–26. https://doi.org/10.1144/GSL.SP.1988.040.01.02.
- Khan, D., Liu, Z.J., Qiu, L.W., Liu, K.Y., Yang, Y.Q., Nie, C., Liu, B., Li, X., Habulashenmu, Y., 2023. Mineralogical and geochemical characterization of lacustrine calcareous shale in Dongying Depression, Bohai Bay Basin: implications for paleosalinity, paleoclimate, and paleoredox conditions. Geochem. (Tokyo. 1967) 83. https://doi.org/10.1016/j.chemer.2023.125978.
- Liang, C., Cao, Y.C., Liu, K.Y., Jiang, Z.X., Wu, J., Hao, F., 2018. Diagenetic variation at the lamina scale in lacustrine organic-rich shales: implications for hydrocarbon migration and accumulation. Geochem. Cosmochim. Acta 229, 112–128. https:// doi.org/10.1016/j.gca.2018.03.017.
- Liu, C.L., Xu, J.L., 2000. Distribution of paleogene coccolithophorids in Jiyang Depression and their relationship with oil and gas. Mar. Geol. Quat. Geol. 20, 73–77. https://doi.org/10.16562/j.cnki.0256-1492.2000.03.012 (in Chinese).
- Liu, C.L., Xu, J.L., Wang, P.X., 2001. Algal blooms: the primary mechanism in the Formation of Lacustrine Petroleum source rocks. Geol. Rev. 47, 207–210. https:// doi.org/10.16509/j.georeview.2001.02.017 (in Chinese).
- Liu, G., Zhou, D.S., 2007. Application of microelements analysis in identifying sedimentary environment—taking Qianjiang formation in the Jianghan basin as an example. Petroleum Geol. Exp. 29, 307–310+314. https://doi.org/10.11781/sysydz200703307 (in Chinese).
- Liu, H.M., Zhang, S., Song, G.Q., Wang, X.J., Teng, J.B., Wang, M., Bao, Y.S., Yao, S.P., Wang, W.Q., Zhang, S.P., Hu, Q.H., Fang, Z.W., 2019. Effect of shale diagenesis on pores and storage capacity in the paleogene Shahejie Formation, dongying depression, Bohai Bay Basin, east China. Mar. Petrol. Geol. 103, 738–752. https://doi.org/10.1016/j.marpetgeo.2019.01.002.
- Liu, S.J., 2019. Sedimentation and its motivation of the Paleogene fine-grained sedimentary rocks in Dongying Sag ——taking the Es4s—Es3x as an example. School of Geosciences. China University of Petroleum (East China), Qingdao, pp. 40—70. https://doi.org/10.27644/d.cnki.gsydu.2019.001656 (in Chinese).
- Liu, Z.L., Xia, B., 2007. Relationship between cenozoic tectonic evolution and plays in Jiyang depression. Nat. Gas Geosci. 18, 209–214+228. https://doi.org/10.1016/S1872-5813(07)60034-6 (in Chinese).
- Livermore, B.D., Dahl, T.W., Bizzarro, M., Connelly, J.N., 2020. Uranium isotope compositions of biogenic carbonates implications for U uptake in shells and the application of the paleo-ocean oxygenation proxy. Geochem. Cosmochim. Acta 287, 50–64. https://doi.org/10.1016/j.gca.2020.07.005.
- Ma, J., Wu, C.D., Wang, Y.Z., Wang, J.L., Fang, Y.N., Zhu, W., Zhai, L.N., Zhou, T.Q., 2017. Paleoenvironmental reconstruction of a saline lake in the Tertiary: evidence from aragonite laminae in the northern Tibet Plateau. Sediment. Geol. 353, 1–12. https://doi.org/10.1016/j.sedgeo.2017.03.002.
- Makeen, Y.M., Hakimi, M.H., Abdullah, W.H., 2015. The origin, type and preservation of organic matter of the Barremian—Aptian organic-rich shales in the Muglad Basin, Southern Sudan, and their relation to paleoenvironmental and paleoclimate conditions. Mar. Petrol. Geol. 65, 187–197. https://doi.org/10.1016/ j.marpetgeo.2015.03.003.
- Marais, D.J.D., Strauss, H., Summons, R.E., Hayes, J.M., 1992. Carbon isotope evidence for the stepwise oxidation of the Proterozoic environment. Nature 359, 605–609. https://doi.org/10.1038/359605a0.
- Martín-García, R., Alonso-Zarza, A.M., Frisia, S., Rodríguez-Berriguete, Á., Drysdale, R., Hellstrom, J., 2019. Effect of aragonite to calcite transformation on the geochemistry and dating accuracy of speleothems. An example from Castañar Cave, Spain. Sediment. Geol. 383, 41–54. https://doi.org/10.1016/

j.sedgeo.2019.01.014.

- McDonough, W.F., Suna, S.S., 1995. The composition of the earth. Chem. Geol. 120, 223–253. https://doi.org/10.1016/0009-2541(94)00140-4.
- Meibom, A., Mostefaoui, S., Cuif, J.P., Dauphin, Y., Houlbreque, F., Dunbar, R., Constantz, B., 2007. Biological forcing controls the chemistry of reef-building coral skeleton. Geophys. Res. Lett. 34. https://doi.org/10.1029/2006GL028657.
- Melim, L., Westphal, H., Swart, P., Eberli, G., Munnecke, A., 2002. Questioning carbonate diagenetic paradigms: evidence from the Neogene of the Bahamas. Mar. Geol. 185, 27–53. https://doi.org/10.1016/S0025-3227(01)00289-4.
- Milliken, K.L., Esch, W.L., Reed, R.M., Zhang, T., 2012. Grain assemblages and strong diagenetic overprinting in siliceous mudrocks, barnett shale (Mississippian), fort worth basin, Texas. AAPG Bull. 96, 1553–1578. https://doi.org/10.1306/ 1201111129
- Milliken, K.L., Olson, T., 2017. Silica diagenesis, porosity evolution, and mechanical behavior in siliceous mudstones, Mowry shale (Cretaceous), Rocky Mountains, U.S.A. J. Sediment. Res. 87, 366–387. https://doi.org/10.2110/jsr.2017.24.
- Milliken, K.L., Zhang, T., Chen, J., Ni, Y., 2021. Mineral diagenetic control of expulsion efficiency in organic-rich mudrocks, Bakken Formation (Devonian-Mississippian), Williston Basin. North Dakota, U.S.A. Mar. Pet. Geol. 127, 104869. https://doi.org/10.1016/j.marpetgeo.2020.104869.
- Miyake, A., Kawano, J., 2010. High-temperature molecular dynamics simulation of aragonite. J. Phys. Condens. Matter 22, 225402. https://doi.org/10.1088/0953-8984/22/22/245402.
- Morse, J., Luther Iii, G., 1999. Chemical influences on trace metal-sulfide interactions in anoxic sediments. Geochem. Cosmochim. Acta 63, 3373–3378. https://doi.org/10.1016/S0016-7037(99)00258-6.
- Munnecke, A., Westphal, H., Reijmer, J.J., Samtleben, C., 1997. Microspar development during early marine burial diagenesis: a comparison of Pliocene carbonates from the Bahamas with Silurian limestones from Gotland (Sweden). Sedimentology 44, 977–990. https://doi.org/10.1111/j.1365-3091.1997.tb02173.x.
- Munnecke, A., Wright, V.P., Nohl, T., 2023. The origins and transformation of carbonate mud during early marine burial diagenesis and the fate of aragonite: A stratigraphic sedimentological perspective. Earth Sci. Rev. 239. https://doi.org/10.1016/j.earscirev.2023.104366.
- Nguyen, A., Gabitov, R., Jimenez, A., Dygert, A., Varco, J., Pérez-Huerta, A., Migdisov, A., Paul, V., Kirkland, B., Dash, P., 2021. Retaining geochemical signatures during aragonite-calcite transformation at hydrothermal conditions. Minerals 11, 1052. https://doi.org/10.3390/min11101052.
- Nohl, T., Steinbauer, M.J., Sinnesael, M., Jarochowska, E., Hollis, C., 2021. Detecting initial aragonite and calcite variations in limestone—marl alternations. Sedimentology 68, 3102—3115. https://doi.org/10.1111/sed.12885.
- Nohl, T., Wetterich, J., Fobbe, N., Munnecke, A., 2020. Lithological dependence of aragonite preservation in monospecific gastropod deposits of the Miocene Mainz Basin: Implications for the (dia-)genesis of limestone—marl alternations. J. Sediment. Res. 90, 1500–1509. https://doi.org/10.2110/jsr.2020.057.
- Oganov, A.R., Glass, C.W., Ono, S., 2006. High-pressure phases of CaCO₃: Crystal structure prediction and experiment. Earth Planet Sci. Lett. 241, 95–103. https://doi.org/10.1016/j.epsl.2005.10.014.
- Pederson, C.L., Mavromatis, V., Dietzel, M., Rollion-Bard, C., Breitenbach, S.F.M., Yu, D., Nehrke, G., Immenhauser, A., 2020. Variation in the diagenetic response of aragonite archives to hydrothermal alteration. Sediment. Geol. 406, 105716. https://doi.org/10.1016/j.sedgeo.2020.105716.
- Peng, J., Yu, L., Xu, T., Wang, Y., Han, H., Pearce, J., 2021. Analysis of Sedimentary Environment Conditions for Lacustrine Fine-Grained Sedimentary Rocks and Its Control of Lithofacies Development: A Case Study of the Lower Submember of Member 3 of Shahejie Formation in FY-1 Well, Dongying Sag, Bohai Bay Basin, China. Geofluids 2021, 1–16. https://doi.org/10.1155/2021/6640706.
- Perrin, C., 2004. Early diagenesis of carbonate biocrystals isomineralogical changes in aragonite coral skeletons. Bull. Soc. Geol. Fr. 175, 95–106. https://doi.org/ 10.2113/175.2.95.
- Phan, T.T., Gardiner, J.B., Capo, R.C., Stewart, B.W., 2018. Geochemical and multiisotopic (⁸⁷Sr/⁸⁶Sr, ¹⁴³Nd/¹⁴⁴Nd, ²³⁸U/²³⁵U) perspectives of sediment sources, depositional conditions, and diagenesis of the Marcellus Shale, Appalachian Basin, USA. Geochem. Cosmochim. Acta 222, 187–211. https://doi.org/10.1016/ i.gca.2017.10.021.
- Pokroy, B., Fitch, A.N., Lee, P.L., Quintana, J.P., Caspi, E.N., Zolotoyabko, E., 2006. Anisotropic lattice distortions in the mollusk-made aragonite: A widespread phenomenon. J. Struct. Biol. 153, 145–150. https://doi.org/10.1016/ j.jsb.2005.10.009.
- Potter, P.E., Maynard, J.B., Depetris, P.J., 2005. Mud and Mudstones: Introduction and Overview. Springer Sci. Bus. Media, pp. 157–174. https://doi.org/10.2113/gsecongeo.100.7.1469.
- Qiu, N.S., Su, X.G., Li, Z.Y., Liu, Z.Q., Li, Z., 2006. The Cenozoic tectono-thermal evolution of Jiyang depression, Bohai bay basin, East China. Chin. J. Geophys. 49, 1127–1135. https://doi.org/10.1002/cjg2.923 (in Chinese).
- Raiswell, R., Fisher, Q.J., 2000. Mudrock-hosted carbonate concretions: a review of growth mechanisms and their influence on chemical and isotopic composition.
 J. Geol. Soc. 157, 239–251. https://doi.org/10.1144/jgs.157.1.239.
 Ramos, F.C., Wolff, J.A., Tollstrup, D.L., 2004. Measuring ⁸⁷Sr/⁸⁶Sr variations in
- Ramos, F.C., Wolff, J.A., Tollstrup, D.L., 2004. Measuring ⁸⁷Sr/⁸⁰Sr variations in minerals and groundmass from basalts using LA-MC-ICPMS. Chem. Geol. 211, 135–158. https://doi.org/10.1016/j.chemgeo.2004.06.025.
- Rask, J.H., Bryndzia, L.T., Braunsdorf, N.R., Murray, T.E., 1997. Smectite illitization in Pliocene-age Gulf of Mexico mudrocks. Clay Clay Miner. 45, 99—109. https://doi.org/10.1346/CCMN.1997.0450112.

- Reeburgh, W.S., 1983. Rates of biogeochemical processes in anoxic sediments. Annu. Rev. Earth Planet Sci. 11, 269—298. https://doi.org/10.1146/annurev.ea.11.050183.001413.
- Reuning, L., Deik, H., Petrick, B., Auer, G., Takayanagi, H., Iryu, Y., Courtillat, M., Bassetti, M.A., Tosca, N., 2022. Contrasting intensity of aragonite dissolution and dolomite cementation in glacial versus interglacial intervals of a subtropical carbonate succession. Sedimentology 2022, 1–19. https://doi.org/10.1111/ sed.12985.
- Riccioni, R.M., Brock, P.W., Schreiber, B.C., 1996. Evidence for early aragonite in paleo-lacustrine sediments. J. Sediment. Res. 66, 1003—1010. https://doi.org/ 10.1306/D4268464-2B26-11D7-8648000102C1865D.
- Robinson, D., Schmidt, S.T., Santana De Zamora, A., 2002. Reaction pathways and reaction progress for the smectite-to-chlorite transformation: Evidence from hydrothermally altered metabasites. J. Metamorph. Geol. 20, 167–174. https://doi.org/10.1046/j.0263-4929.2001.00361.x.
- Roeser, P., Franz, S.O., Litt, T., Ariztegui, D., 2016. Aragonite and calcite preservation in sediments from Lake Iznik related to bottom lake oxygenation and water column depth. Sedimentology 63, 2253–2277. https://doi.org/10.1111/ sed.13306
- Rosenbaum, J., Sheppard, S., 1986. An isotopic study of siderites, dolomites and ankerites at high temperatures. Geochem. Cosmochim. Acta 50, 1147–1150. https://doi.org/10.1016/0016-7037(86)90396-0.
- Rousseau, M., Lopez, E., Stempfle, P., Brendle, M., Franke, L., Guette, A., Naslain, R., Bourrat, X., 2005. Multiscale structure of sheet nacre. Biomaterials 26, 6254–6262. https://doi.org/10.1016/j.biomaterials.2005.03.028.
- Sanders, D., 2003. Syndepositional dissolution of calcium carbonate in neritic carbonate environments: geological recognition, processes, potential significance. J. Afr. Earth Sci. 36. 99–134. https://doi.org/10.1016/S0899-5362(03)00027-7.
- J. Afr. Earth Sci. 36, 99–134. https://doi.org/10.1016/S0899-5362(03)00027-7. Shi, J.Y., Jin, Z.J., Liu, Q.Y., Fan, T.L., Gao, Z.Q., 2021. Sunspot cycles recorded in Eocene lacustrine fine-grained sedimentary rocks in the Bohai Bay Basin, eastern China. Global Planet. Change 205. https://doi.org/10.1016/j.gloplacha.2021.103614.
- Shi, J.Y., Jin, Z.J., Liu, Q.Y., Huang, Z.K., 2020. Depositional process and astronomical forcing model of lacustrine fine-grained sedimentary rocks: A case study of the early Paleogene in the Dongying Sag, Bohai Bay Basin. Mar. Petrol. Geol. 113. https://doi.org/10.1016/j.marpetgeo.2019.08.023.
- Shi, J.Y., Jin, Z.J., Liu, Q.Y., Huang, Z.K., Hao, Y.Q., 2018. Terrestrial sedimentary responses to astronomically forced climate changes during the Early Paleogene in the Bohai Bay Basin, eastern China. Palaeogeogr. Palaeoclimatol. Palaeoecol. 502, 1–12. https://doi.org/10.1016/j.palaeo.2018.01.006.
- Shi, J.Y., Jin, Z.J., Liu, Q.Y., Zhang, T., Fan, T.L., Gao, Z.Q., 2022. Laminar characteristics of lacustrine organic-rich shales and their significance for shale reservoir formation: A case study of the Paleogene shales in the Dongying Sag, Bohai Bay Basin, China. J. Asian Earth Sci. 223. https://doi.org/10.1016/j.jseaes.2021.104976.
- Shiraishi, F., Morikawa, A., Kuroshima, K., Amekawa, S., Yu, T.L., Shen, C.C., Kakizaki, Y., Kano, A., Asada, J., Bahniuk, A.M., 2020. Genesis and diagenesis of travertine, Futamata hot spring, Japan. Sediment. Geol. 405, 105706. https://doi.org/10.1016/j.sedgeo.2020.105706.
- Smrzka, D., Zwicker, J., Misch, D., Walkner, C., Gier, S., Monien, P., Bohrmann, G., Peckmann, J., Tosca, N., 2019. Oil seepage and carbonate formation: A case study from the southern Gulf of Mexico. Sedimentology 66, 2318–2353. https:// doi.org/10.1111/sed.12593.
- Song, C.H., Lu, X.C., Xing, Q., Meng, Q.C., Xia, W.M., Liu, P., Zhang, P., 2007. Late Cenozoic element characters and Palaeoclimatic change of the lacustrine sediments in Linxia Basin, China. Acta Sedimentol. Sin. 25, 409—416. https://doi.org/ 10.3969/j.issn.1000-0550.2007.03.012.
- Song, M.S., 2005. Sedimentary environment geochemistry in the shasi section of southern ramp. Dongying Depression. Miner. Petrol. 25, 67–73. https://doi.org/ 10.19719/j.cnki.1001-6872.2005.01.013 (in Chinese).
- Soto, J.I., Hudec, M.R., Mondol, N.H., Heidari, M., 2021. Shale transformations and physical properties—Implications for seismic expression of mobile shales. Earth Sci. Rev. 220. https://doi.org/10.1016/j.earscirev.2021.103746.
- Steinen, R.P., 1982. SEM observations on the replacement of Bahaman aragonitic mud by calcite. Geology 10, 471–475. https://doi.org/10.1130/0091-7613(1982) 10<471:SOOTRO>2.0.CO:2.
- Steiner, Z., Lazar, B., Reimers, C.E., Erez, J., 2019. Carbonates dissolution and precipitation in hemipelagic sediments overlaid by supersaturated bottom-waters Gulf of Aqaba, Red Sea. Geochem. Cosmochim. Acta 246, 565–580. https://doi.org/10.1016/j.gca.2018.12.007.
- Su, C.P., Li, F., Tan, X.C., Gong, Q.L., Zeng, K., Tang, H., Li, M.L., Wang, X.F., 2020. Recognition of diagenetic contribution to the formation of limestone-marl alternations: A case study from Permian of South China. Mar. Petrol. Geol. 111, 765–785. https://doi.org/10.1016/j.marpetgeo.2019.08.033.

- Swart, P.K., 2015. The geochemistry of carbonate diagenesis: The past, present and future. Sedimentology 62, 1233–1304. https://doi.org/10.1111/sed.12205.
- Tissot, B., Durand, B., Espitali, J., Combaz, A., 1974. Influence of nature and diagenesis of organic matter in formation of petroleum. AAPG Bull. 58, 499–506. https://doi.org/10.1306/83D91425-16C7-11D7-8645000102C1865D.
- Wang, G.M., Xiong, Z.H., Zhang, J., Zhang, B., 2017a. Dissolution experiment and transformation condition analysis of Paleogene aragonite in the Jiyang Depression, China. Aust. J. Earth Sci. 64, 343–352. https://doi.org/10.1080/08120099.2017.1296022.
- Wang, G.M., Xiong, Z.H., Zhang, J., Fu, Y., 2017b. The correspondence between the aragonite content of Palaeogene shale and the thermal evolution of source rocks in Jiyang depression. Acta Petrol. Sin. 38, 855–862. https://doi.org/ 10.7623/syxb201708001 (in Chinese).
- Wang, A.H., Ye, S.Y., Liu, J.K., Ding, X.G., Li, H.L., Xu, N.C., 2020. Discrimination between marine and terrestrial sedimentary environments by the selectively extracted Sr/Ba ratio: A case of sediments in the Yellow River Delta. Acta Sedimentol. Sin. 38, 1226–1238. https://doi.org/10.14027/j.issn.1000-0550.2019.118 (in Chinese).
- Wang, C.L., Liu, C.L., Xu, H.M., Wang, L.C., Shen, L.J., 2013. Sulfur Isotopic Composition of Sulfate and Its Geological Significance of Member 4 of Palaeocene Shashi Formation in Jiangling Depression of Hubei Province. J. Jilin Univ. Earth Sci. Ed. 43, 691–703. https://doi.org/10.13278/ji.cnki.jjuese.2013.03.004 (in Chinese).
- Wanty, R.B., Goldhaber, M.B., 1992. Thermodynamics and kinetics of reactions involving vanadium in natural systems: Accumulation of vanadium in sedimentary rocks. Geochem. Cosmochim. Acta 56, 1471–1483. https://doi.org/ 10.1016/0016-7037(92)90217-7.
- Warren, J.K., 2010. Evaporites through time: Tectonic, climatic and eustatic controls in marine and nonmarine deposits. Earth Sci. Rev. 98, 217–268. https://doi.org/ 10.1016/j.earscirev.2009.11.004.
- Wassenburg, J.A., Immenhauser, A., Richter, D.K., Jochum, K.P., Fietzke, J., Deininger, M., Goos, M., Scholz, D., Sabaoui, A., 2012. Climate and cave control on Pleistocene/Holocene calcite-to-aragonite transitions in speleothems from Morocco: Elemental and isotopic evidence. Geochem. Cosmochim. Acta 92, 23–47. https://doi.org/10.1016/j.gca.2012.06.002.
- Wright, V.P., Cherns, L., 2016. Leaving no stone unturned: the feedback between increased biotic diversity and early diagenesis during the Ordovician. J. Geol. Soc. 173, 241–244. https://doi.org/10.1144/jgs2015-043.
- Wu, G.X., Zhu, W.L., Huang, Z.J., Li, M.B., 1998. Research on phytoplankton and organic matter in the l acustrine sediments and hydrocarbon source conditions. J. Tongji Univ. Nat. Sci. 26, 176–179. https://doi.org/10.1088/0256-307X/15/3/016 (in Chinese).
- Wu, Z.P., Li, W., Ren, Y.J., Lin, C.S., 2003. Basin evolution in the Mesozoic and superposition of Cenozoic Basin in the area of the Jiyang Depression. Acta Geol. Sin. 77, 280–286. https://doi.org/10.3321/j.issn:0001-5717.2003.02.017 (in Chinese).
- Xiong, Z.H., Cao, Y.C., Liang, C., 2024. Characteristics and origin of crystalline dolomite: A case from Paleogene lacustrine fine-grained rocks in Jiyang depression, Bohai Bay Basin, China. Mar. Petrol. Geol. 162, 106694. https:// doi.org/10.1016/j.marpetgeo.2024.106694.
- Xiong, Z.H., Cao, Y.C., Liang, C., Liu, K.Y., Wang, G.M., Zhu, R., Lei, P., Wang, Y.L., 2022. Origin and significance of authigenic quartz and albite in lacustrine calcareous fine-grained sedimentary rocks. Mar. Petrol. Geol. 143, 105799. https://doi.org/ 10.1016/j.marpetgeo.2022.105799.
- Zhang, J.G., Jiang, Z.X., Liang, C., Wu, J., Xian, B.Z., Li, Q., 2016. Lacustrine massive mudrock in the Eocene Jiyang Depression, Bohai Bay Basin, China: Nature, origin and significance. Mar. Petrol. Geol. 77, 1042–1055. https://doi.org/ 10.1016/j.marpetgeo.2016.08.008.
- Zhang, Y.S., Yang, Y.Q., Qi, Z.X., Qiao, Y.D., Yuan, H.R., 2003. Sedimentary characteristics and environments of the salt-bearing series of Qianjiang formation of the paleogene in Qianjiang sag of Jianghan Basin. J. Palaeogeogr. 5, 29–35. https://doi.org/10.3969/j.issn.1671-1505.2003.01.003 (in Chinese).
- Zhong, X.C., Zhong, S.L., Fei, X.D., Nie, Y.S., Lin, T., 1988. Calcareous nannofossils from the Oligocene Shahejie Member in the Bohai Basin and their sedimentary environment. Acta Micropalaeontol. Sin. 5, 145–151. CNKI:SUN:WSGT.0.1988-02-002 (in Chinese).
- Zhu, X.M., Zhang, M.Z., Zhu, S.F., Dong, Y.L., Li, C., Bi, Y.Q., Ma, L.C., 2022. Shale Lithofacies and Sedimentary Environment of the Third Member, Shahejie Formation, Zhanhua Sag, Eastern China. Acta Geol. Sin. - Engl. Ed. 96, 1024–1040. https://doi.org/10.1111/1755-6724.14804.
- Zwicker, J., Smrzka, D., Himmler, T., Monien, P., Gier, S., Goedert, J.L., Peckmann, J., 2018. Rare earth elements as tracers for microbial activity and early diagenesis: A new perspective from carbonate cements of ancient methane-seep deposits. Chem. Geol. 501, 77–85. https://doi.org/10.1016/j.chemgeo.2018.10.010.